

Hole statistics and superfluid phases in quantum dimer models

C. A. Lamas,¹ A. Ralko,² M. Oshikawa,³ D. Poilblanc,¹ and P. Pujol¹

¹*Laboratoire de Physique Théorique, IRSAMC, CNRS and Université de Toulouse, UPS, F-31062 Toulouse, France*

²*Institut Néel, CNRS and Université Joseph Fourier, F-38042 Grenoble, France*

³*Institute for Solid State Physics, University of Tokyo, Kashiwa 277-8581, Japan*

(Received 18 October 2012; published 12 March 2013)

Quantum dimer models (QDMs) arise as low-energy effective models for frustrated magnets. Some of these models have proven successful in generating a scenario for exotic spin liquid phases with deconfined spinons. Doping, i.e., the introduction of mobile holes, has been considered within the QDM framework and partially studied. A fundamental issue is the possible existence of a superconducting phase in such systems and its properties. For this purpose, the question of the statistics of the mobile holes (or “holons”) shall be addressed first. Such issues are studied in detail in this paper for generic doped QDMs defined on the most common two-dimensional lattices (square, triangular, honeycomb, kagome, . . .) and involving general resonant loops. We prove a general “statistical transmutation” symmetry of such doped QDMs by using composite operators of dimers and holes. This exact transformation enables us to define duality equivalence classes (or families) of doped QDMs, and provides the analytic framework to analyze dynamical statistical transmutations. We discuss various possible superconducting phases of the system. In particular, the possibility of an exotic superconducting phase originating from the condensation of (bosonic) charge- e holons is examined. A numerical evidence of such a superconducting phase is presented in the case of the triangular lattice, by introducing a gauge-invariant holon Green’s function. We also make the connection with a Bose-Hubbard model on the kagome lattice which gives rise, as an effective model in the limit of strong interactions, to a doped QDM on the triangular lattice.

DOI: [10.1103/PhysRevB.87.104512](https://doi.org/10.1103/PhysRevB.87.104512)

PACS number(s): 67.80.bd, 74.20.Mn, 05.30.-d, 75.10.Kt

I. INTRODUCTION

In 1987 Anderson¹ suggested that the strange behavior of cuprate materials between the superconducting dome and the magnetically ordered insulating phase could be described by a resonating valence bond (RVB) state in which preexisting magnetic singlet pairs of the insulating state become charged superconducting pairs when the insulator is doped. Just one year later appeared the first effective model in which the magnetic degrees of freedom are disregarded in favor of the more pertinent singlet degrees of freedom.² This is nothing but the quantum dimer model (QDM). However, it was soon realized³ that the ground state of the undoped $S = 1/2$ Heisenberg antiferromagnet on a square lattice exhibits a long-range Néel order in contrast to the initial expectation based on the RVB picture. Furthermore, the QDM on a square lattice was also found to have only gapped crystalline phases but no evidence of an RVB spin liquid phase in a finite region of the phase diagram.⁴ It is still possible to argue that, even though the undoped antiferromagnet has the Néel order, the RVB picture gives a better theoretical starting point once the system is doped with holes. However, it would be natural to ask if the RVB spin liquid phase can be realized in undoped magnetic system with only short-range interaction.

One may expect that magnetic frustration would favor the RVB state over the Néel phase. Thus, over time, the main interest in the QDM was shifted from the original motivation of the application to high- T_c superconductivity, to the effects of frustration. However, clear confirmation of a RVB phase remained elusive for a rather long time. A breakthrough in the study of the QDM was due to Moessner and Sondhi⁵ who showed that a simple QDM defined in the triangular lattice exhibit a disordered phase which, recalling that these dimer models are supposed to be effective models for frustrated

magnets, can be considered as an explicit example of the RVB spin liquid phase. It was also recognized that the RVB spin liquid phase is a topologically ordered phase with a nontrivial topological degeneracy of the ground states.⁶ In fact, the RVB spin liquid phase is essentially identical to the \mathbb{Z}_2 topological phase which was introduced in a completely different context of quantum information processing.⁷ The QDM is generally not exactly equivalent to an antiferromagnetic Hamiltonian defined in terms of quantum spins. However, the projection from a magnetic system to a QDM was performed successfully in Heisenberg antiferromagnets on frustrated lattices, such as the square lattice with strong enough second and/or third neighbors couplings^{8,9} or the kagome lattice.¹⁰ These suggest that the QDM may well represent phases without magnetic order in antiferromagnets. In fact, very recently, frustrated Heisenberg antiferromagnets on kagome and other lattices are reported to be in the RVB spin liquid phase (\mathbb{Z}_2 topological phase) by several authors.^{11–13}

Now that the existence of the RVB spin liquid phase appears to be confirmed in QDMs as well as in antiferromagnets, the issue of superconductivity in doped spin liquids becomes a more pressing question. This issue started in fact to be investigated shortly after the appearance of the QDM.¹⁴ Doping of an RVB spin liquid is expected to induce a novel type of elementary excitations called holon. A holon, carrying electric charge e but no spin, appears as a result of fractionalization, namely deconfinement of fractionalized excitations. Indeed, topological degeneracy of the undoped RVB spin liquid is known to be intimately connected to the fractionalization phenomenon.¹⁵

Superconductivity may be realized if the holons condense. At least naively, one may expect that the resulting superconductor is an exotic one due to condensation of charge- e holons, instead of usual charge- $2e$ Cooper pairs. A fundamental

issue in this problem is the statistics of the holon. For the holons to condense without forming pairs, they must be bosons. However, it should be noted that transmutation of the statistics^{16,17} is possible. Namely, the statistics of holons as elementary excitations appearing in the low-energy limit can be different from the statistics assigned to holes in the microscopic model.

In this paper we address the issue of the statistics of holes and its interplay with possible superconducting phases in doped QDMs. In a recent work¹⁸ it was shown that a QDM with fermionic (at microscopic level) holes is equivalent to another QDM with bosonic holes. Because of the equivalence, the statistics of the holon as a physical elementary excitation must be the same for either representation. This proves the existence of a dynamical statistical transmutation in the system. In this paper we study in more detail the statistical transmutation in QDMs and give a simple and efficient method to obtain the relation between the QDMs with fermionic and bosonic representation of the holes.

In Sec. II we introduce a second quantization notation for QDM Hamiltonians and show the gauge symmetry associated with them. In Sec. III we present the composite particle representation of QDM Hamiltonians which is the key ingredient to show the exact equivalence between a QDM with bosonic and another QDM with fermionic holes. This equivalence is shown for a generic flipping term defined in any kind of lattice. The result, which relies on an orientation prescription of the bonds in the lattice considered, is totally generic and can then be applied to any QDM defined in the most common lattices. The method used here differs considerably from, and has numerous advantages over, the one used in Ref. 18 where a two-dimensional version of the Jordan-Wigner (JW) transformation was used. In Sec. IV we argue how the modification of the orientation prescription can be interpreted as a simple gauge transformation in the QDM Hamiltonian. We then apply the general result of the statistical transmutation obtained in Sec. III to generic QDM Hamiltonians defined on the square, triangular, hexagonal, and kagome lattices. Section V is devoted to numerical investigation of four inequivalent QDMs defined on the triangular lattice. In particular, we identify an exotic superconductor phase due to condensation of holons with charge e , measuring numerically the gauge-invariant Green's function of a single holon. In Sec. VI we discuss an explicit realization of one of the QDMs discussed in Sec. V. It is obtained as a low-energy strong interaction limit of a Bose-Hubbard model on the kagome lattice. The number of bosons is directly related to the doping, or number of holes, in the resulting QDM on the triangular lattice. Section VII is devoted to the discussion of our results. We also include as an appendix the derivation of the statistical transmutation for a generic QDM on the kagome lattice using the Jordan-Wigner transformation. Of course the result is consistent with the one obtained with the composite particle representation obtained in Sec. III, but allows a better understanding of the connection between these two different methods.

II. THE HAMILTONIAN AND ITS GAUGE SYMMETRIES

We start with a doped quantum dimer model on a two-dimensional lattice. To fix the ideas, we work here with the

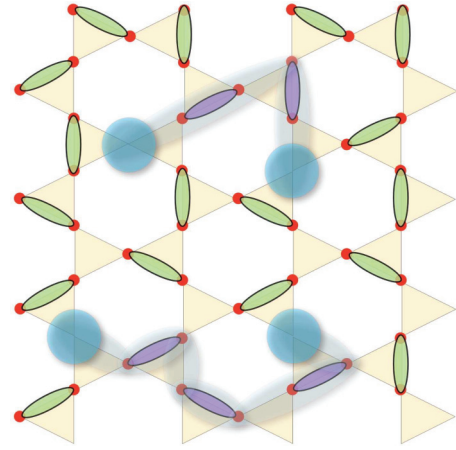


FIG. 1. (Color online) Schematic snapshot of a doped “dimer liquid”. Each site is occupied by either a (single) dimer or a hole (empty site).

Hamiltonian defined on the square lattice but all the arguments remain valid for any two-dimensional lattice. We write the Hamiltonian as

$$H = H_J + H_V + H_t \quad (1)$$

with

$$\begin{aligned} H_J &= -J \sum_{\square} [| \begin{smallmatrix} \bullet & \bullet \\ \bullet & \bullet \end{smallmatrix} \rangle \langle \begin{smallmatrix} \bullet & \bullet \\ \bullet & \bullet \end{smallmatrix} | + \text{H.C}] \\ H_V &= V \sum_{\square} [| \begin{smallmatrix} \bullet & \bullet \\ \bullet & \bullet \end{smallmatrix} \rangle \langle \begin{smallmatrix} \bullet & \bullet \\ \bullet & \bullet \end{smallmatrix} | + | \begin{smallmatrix} \bullet & \bullet \\ \bullet & \bullet \end{smallmatrix} \rangle \langle \begin{smallmatrix} \bullet & \bullet \\ \bullet & \bullet \end{smallmatrix} |] \\ H_t &= -t \sum_{\square} \{ | \begin{smallmatrix} \bullet & \bullet \\ \bullet & \circ \end{smallmatrix} \rangle \langle \begin{smallmatrix} \bullet & \circ \\ \bullet & \bullet \end{smallmatrix} | + | \begin{smallmatrix} \bullet & \circ \\ \bullet & \bullet \end{smallmatrix} \rangle \langle \begin{smallmatrix} \bullet & \bullet \\ \bullet & \circ \end{smallmatrix} | \\ &+ | \begin{smallmatrix} \bullet & \circ \\ \bullet & \bullet \end{smallmatrix} \rangle \langle \begin{smallmatrix} \circ & \bullet \\ \bullet & \bullet \end{smallmatrix} | + | \begin{smallmatrix} \circ & \bullet \\ \bullet & \bullet \end{smallmatrix} \rangle \langle \begin{smallmatrix} \bullet & \bullet \\ \circ & \bullet \end{smallmatrix} | + \text{H.C} \}, \end{aligned}$$

where the sums are over all the smallest resonant plaquettes on the lattice (for the square lattice these are the squares). In a second quantized formalism we assume that dimer configurations are created by spatially symmetric dimer operators $b_{i,j}^\dagger$ and holes are created by bosonic operators a_k^\dagger (see Fig. 1). Then, we can rewrite the Hamiltonian as

$$H_J = -J \sum_{\square} \{ b_{i,j}^\dagger b_{j,k}^\dagger b_{j,k} b_{l,i} + \text{H.c.} \}, \quad (2)$$

$$H_V = V \sum_{\square} \{ b_{i,j}^\dagger b_{k,l}^\dagger b_{i,j} b_{k,l} + b_{j,k}^\dagger b_{l,i}^\dagger b_{j,k} b_{l,i} \}, \quad (3)$$

$$H_t = -t \sum_i \{ b_{i,j}^\dagger b_{j,k} a_k^\dagger a_i + \text{H.c.} \}. \quad (4)$$

In the last equation, the indices correspond to the labeling of the sites of a square plaquette as in Fig. 2. In our previous conventions, dimer configurations are represented by spatially symmetric operators $b_{i,j}^\dagger$ satisfying

$$[b_{i,j}, b_{k,l}^\dagger] = \delta_{i,k} \delta_{j,l} + \delta_{i,l} \delta_{j,k}, \quad [b_{i,j}, b_{k,l}] = [b_{i,j}^\dagger, b_{k,l}^\dagger] = 0. \quad (5)$$

The boson operator a_i^\dagger creates a hole in the site i and satisfies

$$[a_i, a_j^\dagger] = \delta_{i,j}, \quad [a_i, a_j] = [a_i^\dagger, a_j^\dagger] = 0. \quad (6)$$

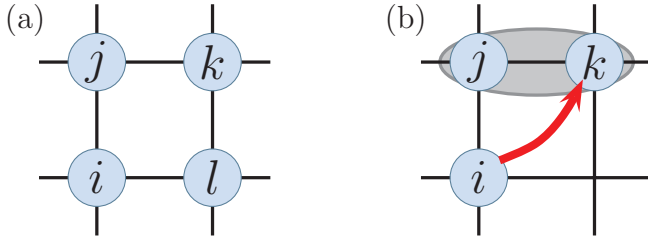


FIG. 2. (Color online) (a) Indexes corresponding to each square plaquette in the Hamiltonians H_J and H_V . (b) Indexes corresponding to each hopping process in H_t .

The operators a and b commute one with each other,

$$[a_i, b_j] = [a_i^\dagger, b_j^\dagger] = [a_i^\dagger, b_j] = 0. \quad (7)$$

We introduce in the model a constraint on the number of dimers and holes which warrants that at each site of the lattice there is either one and only one hole or one and only one dimer arriving to it:

$$a_i^\dagger a_i + \sum_{z=\pm\hat{e}_1, \pm\hat{e}_2} b_{i,i+z}^\dagger b_{i,i+z} = 1. \quad (8)$$

Of course this constraint implies, among others, that the holes have to be considered as hard-core bosons. It is important to notice that the Hamiltonian has the following U(1) gauge symmetry:

$$a_j \rightarrow e^{i\xi_j} a_j, \quad (9)$$

$$b_{j,k} \rightarrow e^{i(\xi_j + \xi_k)} b_{j,k}, \quad (10)$$

where ξ_i is an angle. This invariance can be exploited to prove the statistical transmutation symmetry in some two-dimensional systems by means of a Jordan-Wigner transformation on the holon operators.¹⁸ In the following we present an alternative description for the doped QDM using composite operators which allows us to understand in a different way the equivalence between a model with bosonic holes and one with fermionic holes. For doing this, we have first to make a choice of a given orientation prescription for the bonds in the lattice.

III. THE ‘‘COMPOSITE’’ REPRESENTATION FOR THE QDM

A. Composite particles

In order to prove the equivalence between a QDM Hamiltonian with bosonic holes and another Hamiltonian with fermionic holes, we propose a different formulation for the QDM. This formulation is done in terms of composite particles by defining the operator

$$B_{i,j} = b_{i,j} a_i^\dagger a_j^\dagger. \quad (11)$$

This operator destroys a dimer between sites i and j and creates two holes at the same sites. Let us call \mathcal{H}_c the subspace of states that satisfies the constraint (8). For a given state $|\psi\rangle \in \mathcal{H}_c$ we have that $|\tilde{\psi}\rangle = B_{i,j}|\psi\rangle$ is also a vector in \mathcal{H}_c .

One can easily notice that the operator $B_{i,j}$ is invariant under the gauge transformation (9) and (10). This U(1) gauge symmetry was exploited in Ref. 14 to represent a doped QDM

as a gauge theory coupled to a matter field. More importantly, one can check that *within the subspace* \mathcal{H}_c , the set of operators $\{B_{i,j}\}$ form a closed algebra similar to the one of $\{b_{i,j}\}$. The Hamiltonian can entirely be written in terms of these $B_{i,j}$ operators making its gauge invariance manifest. Its precise form is given by $H = H_J + H_V + H_t$ with

$$H_J = -J \sum_{\square} \{B_{i,j}^\dagger B_{k,l}^\dagger B_{j,k} B_{l,i} + \text{H.c.}\}, \quad (12)$$

$$H_V = V \sum_{\square} \{B_{i,j}^\dagger B_{k,l}^\dagger B_{i,j} B_{k,l} + B_{j,k}^\dagger B_{l,i}^\dagger B_{j,k} B_{l,i}\}, \quad (13)$$

$$H_t = -t \sum_i \{B_{i,j}^\dagger B_{j,k} + \text{H.c.}\}. \quad (14)$$

It is evident that, within this formulation, the basic building blocks of the model are created by $B_{i,j}^\dagger$ which corresponds to composite particles of charge $2e$. Namely, the model is completely defined in terms of the constituent particle with charge $2e$. This has several important consequences. In particular, the gauge invariance requires that the energy spectrum of the system on a torus, as a function of the magnetic flux Φ through the ‘‘hole’’ of the torus, is invariant under $\Phi \rightarrow \Phi + \pi/e$. (For early discussions on the π/e -flux periodicity in the QDMs, see Refs. 19 and 20 and references therein.) This periodicity corresponds to the unit flux quantum for charge $2e$ objects. However, this does not necessarily mean that the physical elementary excitations of the system have minimum charge $2e$.¹⁵ The system can have a topological order which leads to *fractionalization*; elementary excitations can have fractions of the charge $2e$ of the constituent particle of the microscopic Hamiltonian. If the charge- e holons are deconfined as a result of fractionalization, they could condense to form an exotic superconductor.

The apparent contradiction between the periodicity of the energy spectrum in π/e flux and the expected flux quantization in the unit of $2\pi/e$ in the condensate of charge- e holons is resolved by the existence of the topological vortex excitation called vison. Insertion of the π/e flux corresponds to trapping of a vison. Although the flux periodicity of the ground-state energy does not distinguish an exotic charge- e condensate from the usual superconductor, an experimental detection scheme of the charge- e condensation, based on a ‘‘vortex memory effect’’, was proposed.²¹ An actual experiment²² on the high- T_c superconductor did not find such a signature of charge- e condensation. Nevertheless, the exotic superconductivity due to condensation of charge- e objects is possible in principle, and is an interesting subject to pursue theoretically and experimentally. Later in this paper, we will introduce a quantity which detects a charge- e condensation, and study it numerically in several QDMs.

B. Statistical transmutation symmetry

One of the main advantages of the formulation in terms of composite operators presented above is that one can prove an equivalence between a Hamiltonian where holes are hard-core bosons and another one where the holes are fermions. Let us consider a QDM Hamiltonian with bosonic holes, where their creation and annihilation operators a_i^\dagger and a_j satisfy bosonic commutation relations. Let us also consider another QDM Hamiltonian with fermionic holes, created and

annihilated by the set of operators f_i^\dagger and f_j which now satisfy fermionic anticommutation relations. We then build the respective composite operators:

$$B_{i,j} = b_{i,j} a_i^\dagger a_j^\dagger, \quad (15)$$

$$\tilde{B}_{i,j} = b_{i,j} f_i^\dagger f_j^\dagger. \quad (16)$$

As for the operators \tilde{B} , in the rest of the paper all quantities with a tilde correspond to operators and coupling constants of the *fermionic* representation for the holes. Before proceeding, there is an important statement to make. Again, one can show that within the subspace \mathcal{H}_c , both set of operators $\{B_{i,j}\}$ and $\{\tilde{B}_{i,j}\}$ form the *same* closed algebra of *bosonic* dimer operators. Another important point is that the definition of the composite operators in terms of fermions is more subtle because it is necessary to take a prescription for the orientation of the dimers (which determines the order of the fermions in the endpoints of each dimer).

In the following we will call “even prescription” of a given plaquette an ordering prescription for the bonds such that all the bonds are oriented in a clockwise direction or an even number of bonds are oriented anticlockwise. By contrast we call “odd prescription” the prescriptions obtained from the clockwise ordering by flipping an odd number of bonds.

Notice that, since the resonance plaquettes containing N dimers have necessary $2N$ bonds, the anticlockwise prescription (where all bonds are oriented anticlockwise) is always an *even prescription*.

Theorem. Given a resonant plaquette of arbitrary length with an even prescription for the bonds, then, for the kinetic term of the dimers in the plaquette, we have the equivalence $H_J(J, \text{bosons}) \leftrightarrow H_J(-J, \text{fermions})$. In other words, the resonance term of dimers in the plaquette is invariant under a simultaneous change of “statistics” of the holes in the system (i.e., bosonic into fermionic or vice versa) and the sign of the dimer resonance loop amplitude J .

Proof. Consider a resonance loop containing $2N$ sites (N dimers) numbered from 1 to $2N$ in the clockwise direction as in Figs. 3(a) and 3(b). The kinetic Hamiltonian for dimers belonging to this loop can be written in terms of bond operators $b_{i,j}$ as

$$H_J^N = J[b_{1,2}^\dagger b_{3,4}^\dagger b_{5,6}^\dagger \cdots b_{2N-3,2N-2}^\dagger b_{2N-1,2N}^\dagger] \times [b_{2,3} b_{4,5} \cdots b_{2N-2,2N-1} b_{2N,1}] + \text{H.c.}, \quad (17)$$

where the index N indicates the number of dimers in the loop.

Now, we add one dimer (two sites) to the loop, obtaining a resonance loop with $N+1$ dimers. In this case, the

Hamiltonian can be written as

$$H_J^{N+1} = J[b_{1,2}^\dagger b_{3,4}^\dagger b_{5,6}^\dagger \cdots b_{2N-3,2N-2}^\dagger b_{2N-1,2N}^\dagger b_{\alpha,\beta}^\dagger] \times [b_{2,3} b_{4,5} \cdots b_{2N-2,2N-1} b_{2N,\alpha} b_{\beta,1}] + \text{H.c.}$$

Since all the operators are acting on different bonds they all commute and we can rearrange them in the following way:

$$\begin{aligned} H_J^N &= J[b_{1,2}^\dagger b_{3,4}^\dagger \cdots b_{2N-3,2N-2}^\dagger b_{2N-1,2N}^\dagger] \\ &\quad \times [b_{2,3} b_{4,5} \cdots b_{2N-2,2N-1}] b_{2N,1} + \text{H.c.}, \\ H_J^{N+1} &= J[b_{1,2}^\dagger b_{3,4}^\dagger \cdots b_{2N-3,2N-2}^\dagger b_{2N-1,2N}^\dagger] \\ &\quad \times [b_{2,3} b_{4,5} \cdots b_{2N-2,2N-1}] b_{\alpha,\beta}^\dagger b_{2N,\alpha} b_{\beta,1} + \text{H.c.}, \end{aligned}$$

or in a compact notation,

$$\begin{aligned} H_J^N &= J \left(\prod_{j=1}^N b_{2j-1,2j}^\dagger \right) \left(\prod_{j=1}^{N-1} b_{2j,2j+1} \right) b_{2N,1} + \text{H.c.}, \\ H_J^{N+1} &= J \left(\prod_{j=1}^N b_{2j-1,2j}^\dagger \right) \left(\prod_{j=1}^{N-1} b_{2j,2j+1} \right) b_{\alpha,\beta}^\dagger b_{2N,\alpha} b_{\beta,1} \\ &\quad + \text{H.c.} \end{aligned}$$

Now, we insert on the right of the Hamiltonian the string of operators $S_N^f = \prod_{i=1}^{2N} f_i f_i^\dagger$, where the index i corresponds to the sites on the resonance loop. This operator acts as the identity operator on the sites belonging to the loop because $f_i f_i^\dagger = 1$ in the absence of holes. We start with the Hamiltonian H_J^N :

$$\begin{aligned} H_J^N &= H_J^N S_N^f = J \left(\prod_{j=1}^N b_{2j-1,2j}^\dagger \right) \left(\prod_{j=1}^{N-1} b_{2j,2j+1} \right) b_{2N,1} \\ &\quad \times f_1 f_1^\dagger \cdots f_{2N} f_{2N}^\dagger + \text{H.c.} \end{aligned}$$

Now, we move the fermions to the left in order to form the composite operators $\tilde{B}_{i,j} = b_{i,j} f_i^\dagger f_j^\dagger$ corresponding to the dimer operators inside the brackets. Commutation of the fermions gives a global sign,

$$\begin{aligned} H_J^N &= (-1)^\xi J \left(\prod_{j=1}^N \tilde{B}_{2j-1,2j}^\dagger \right) \left(\prod_{j=1}^{N-1} \tilde{B}_{2j,2j+1} \right) \\ &\quad \times b_{2N,1} f_1^\dagger f_{2N}^\dagger + \text{H.c.} \end{aligned}$$

We can follow exactly the same procedure in the loop with $N+1$ dimers; the global sign resulting from the commutation of fermion operators to write the products in terms of composite

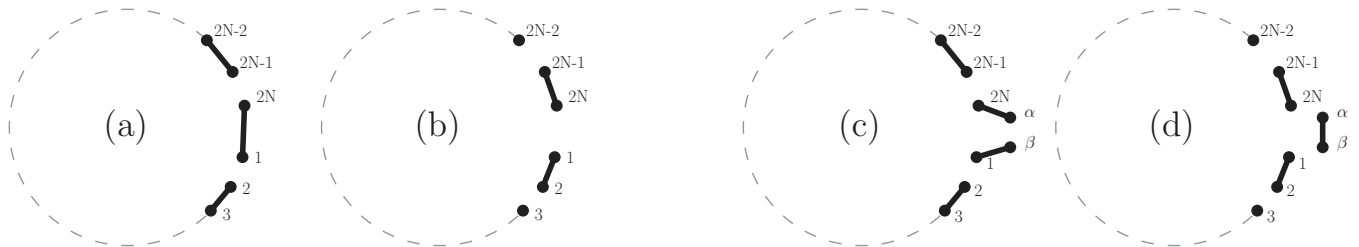


FIG. 3. Elements used to prove the inductive step. Panels (a) and (b) correspond to the two possible dimerizations in a N dimers plaquette whereas (c) and (d) correspond to the plaquette with $N+1$ dimers.

particles is the same as that in the N dimers case. We can write for the $N + 1$ case,

$$H_j^{N+1} = (-1)^\xi J \left(\prod_{j=1}^N \tilde{B}_{2j-1,2j}^\dagger \right) \left(\prod_{j=1}^{N-1} \tilde{B}_{2j,2j+1} \right) \times b_{\alpha,\beta}^\dagger b_{2N,\alpha} b_{\beta,1} f_1^\dagger f_{2N}^\dagger f_\alpha f_\beta f_\beta^\dagger f_\alpha^\dagger + \text{H.c.}$$

Now we can determine the change in the sign of J when a dimer is added in the loop. First we commute the operators f_1^\dagger and f_{2N}^\dagger in H_j^N to form the operator $\tilde{B}_{2N,1} = b_{2N,j,1} f_{2N}^\dagger f_1^\dagger$. This commutation gives another sign to complete the global phase in the Hamiltonian. Then we can write for the N dimers case

$$H_j^N = (-1)^{\xi+1} J \left(\prod_{j=1}^N \tilde{B}_{2j-1,2j}^\dagger \right) \left(\prod_{j=1}^{N-1} \tilde{B}_{2j,2j+1} \right) \tilde{B}_{2N,1} + \text{H.c.}$$

In the Hamiltonian corresponding to $N + 1$ dimers we have to define three composite operators. We have that

$$b_{\alpha,\beta}^\dagger b_{2N,\alpha} b_{\beta,1} f_1^\dagger f_{2N}^\dagger f_\alpha f_\beta f_\beta^\dagger f_\alpha^\dagger = (b_{\alpha,\beta}^\dagger f_\beta f_\alpha) b_{2N,\alpha} b_{\beta,1} f_1^\dagger f_{2N}^\dagger f_\alpha f_\beta^\dagger \quad (18)$$

$$= (b_{\alpha,\beta}^\dagger f_\beta f_\alpha) (b_{2N,\alpha} f_{2N}^\dagger f_\alpha) b_{\beta,1} f_1^\dagger f_\beta^\dagger \quad (19)$$

$$= (-1) (b_{\alpha,\beta}^\dagger f_\beta f_\alpha) (b_{2N,\alpha} f_{2N}^\dagger f_\alpha) (b_{\beta,1} f_1^\dagger f_\beta^\dagger) \quad (20)$$

$$= (-1) \tilde{B}_{\alpha,\beta}^\dagger \tilde{B}_{2N,\alpha} \tilde{B}_{\beta,1}. \quad (21)$$

Finally, the Hamiltonian corresponding to $N + 1$ dimers reads

$$H_j^{N+1} = (-1)^{\xi+1} J \left(\prod_{j=1}^N \tilde{B}_{2j-1,2j}^\dagger \right) \left(\prod_{j=1}^{N-1} \tilde{B}_{2j,2j+1} \right) \times \tilde{B}_{\alpha,\beta}^\dagger \tilde{B}_{2N,\alpha} \tilde{B}_{\beta,1} + \text{H.c.}$$

We have proved by induction that, if for a N dimers loop, the kinetic term acquires a given sign when the Hamiltonian is written in terms of fermionic composite particles, then the kinetic amplitude corresponding to $N + 1$ dimers acquires the same sign. To complete this mathematical induction proof we need check that the statement holds for the lowest value of N . The smallest possible resonance loop is given by a loop with only two dimers. It is easy to check that in this case

$$\begin{aligned} H_j^2 &= J b_{1,2}^\dagger b_{3,4}^\dagger b_{2,3} b_{4,1} + \text{H.c.} \\ &= J b_{1,2}^\dagger b_{3,4}^\dagger b_{2,3} b_{4,1} f_1^\dagger f_2^\dagger f_2 f_3 f_3^\dagger f_4 f_4^\dagger + \text{H.c.} \\ &= (-1) J \tilde{B}_{1,2}^\dagger \tilde{B}_{3,4}^\dagger \tilde{B}_{2,3} \tilde{B}_{4,1} + \text{H.c.} \end{aligned}$$

Then we have proved that the kinetic term for a resonance loop of arbitrary length oriented in a clockwise direction, the amplitude J in the Hamiltonian written using dimer operators $b_{i,j}$, changes to $-J$ when we write the Hamiltonian in terms of fermionic composite operators $\tilde{B}_{i,j}$. A trivial verification shows that the amplitude remains unchanged when we write the Hamiltonian in terms of bosonic operators $B_{i,j} = b_{i,j} a_i^\dagger a_j^\dagger$.

The result above can be rewritten in the more appealing way:

$$H_j(J, \tilde{B}) \equiv H_j(-J, B). \quad (22)$$

The proof can easily be extended to the potential term H_V . In this case it is easy to see that the bosonic and fermionic versions give the same sign in the amplitude V ,

$$H_V(V, \tilde{B}) \equiv H_V(V, B). \quad (23)$$

The equivalence proved above is valid for any even prescription on the plaquette. Starting from the clockwise prescription where the results above have been proved, if we flip two bonds this induces the commutation of two fermionic operators and the sign remains unchanged. But if we flip an odd number of loops we must commute an odd number of extra fermionic commutations in order to form the composite operators. These permutations give an extra sign in the Hamiltonian. Then it is easy to prove the following corollary:

Corollary 1. Given a resonant plaquette of arbitrary length with an odd prescription for the bonds, then, for the kinetic energy of the dimers in the plaquette, we have the equivalence $H_J(J, \text{bosons}) \leftrightarrow H_J(J, \text{fermions})$.

The equivalence in the potential term does not change if we take an odd or even prescription. Using this property of the potential term and Corollary 1 we can derive the following corollary.

Corollary 2. Note that we have actually proved that, if in a given lattice we can take an even prescription for all the plaquettes involved in the Hamiltonian, then the equivalence

$$H(J, V, \text{bosons}) \equiv H(-J, V, \text{fermions}) \quad (24)$$

is valid for the Hamiltonian in the complete lattice, whereas if we can take an odd prescription for all the plaquettes in the Hamiltonian, we have the equivalence

$$H(J, V, \text{bosons}) \equiv H(J, V, \text{fermions}). \quad (25)$$

In order to complete the panorama for the doped QDM we study the fermionic and bosonic representation of the Hamiltonian H_t corresponding to the hopping of holes.

Consider three nearest-neighbors sites of the lattice as in Fig. 2(b). In terms of bosonic holes and dimer operators we can write a general hopping term as

$$h_{i,j,k}^{(t)} = b_{i,j}^\dagger b_{j,k} a_k^\dagger a_i \quad (26)$$

if there is no hole in the intermediate site j we can add on the right the identity as $a_j a_j^\dagger = 1$. We then obtain

$$h_{i,j,k}^{(t)} = -t b_{i,j}^\dagger b_{j,k} a_k^\dagger a_i a_j a_j^\dagger \quad (27)$$

$$= -t (b_{i,j}^\dagger a_j a_i) (b_{j,k} a_j^\dagger a_k^\dagger) \quad (28)$$

$$= -t B_{i,j}^\dagger B_{j,k}. \quad (29)$$

In the bosonic case we do not need to worry about the prescription in the lattice but it is important when we study the fermionic description. In this case we take the prescription $i \rightarrow j \rightarrow k$. Starting from the Hamiltonian

$$\tilde{h}_{i,j,k}^{(t)} = b_{i,j}^\dagger b_{j,k} f_k^\dagger f_i \quad (30)$$

we insert on the right the operators $f_j f_j^\dagger = 1$,

$$\tilde{h}_{i,j,k}^{(t)} = -t b_{i,j}^\dagger b_{j,k} f_k^\dagger f_i f_j f_j^\dagger \quad (31)$$

$$= -t (b_{i,j}^\dagger f_j f_i) (b_{j,k} f_j^\dagger f_k^\dagger) \quad (32)$$

$$= -t \tilde{B}_{i,j}^\dagger \tilde{B}_{j,k}. \quad (33)$$

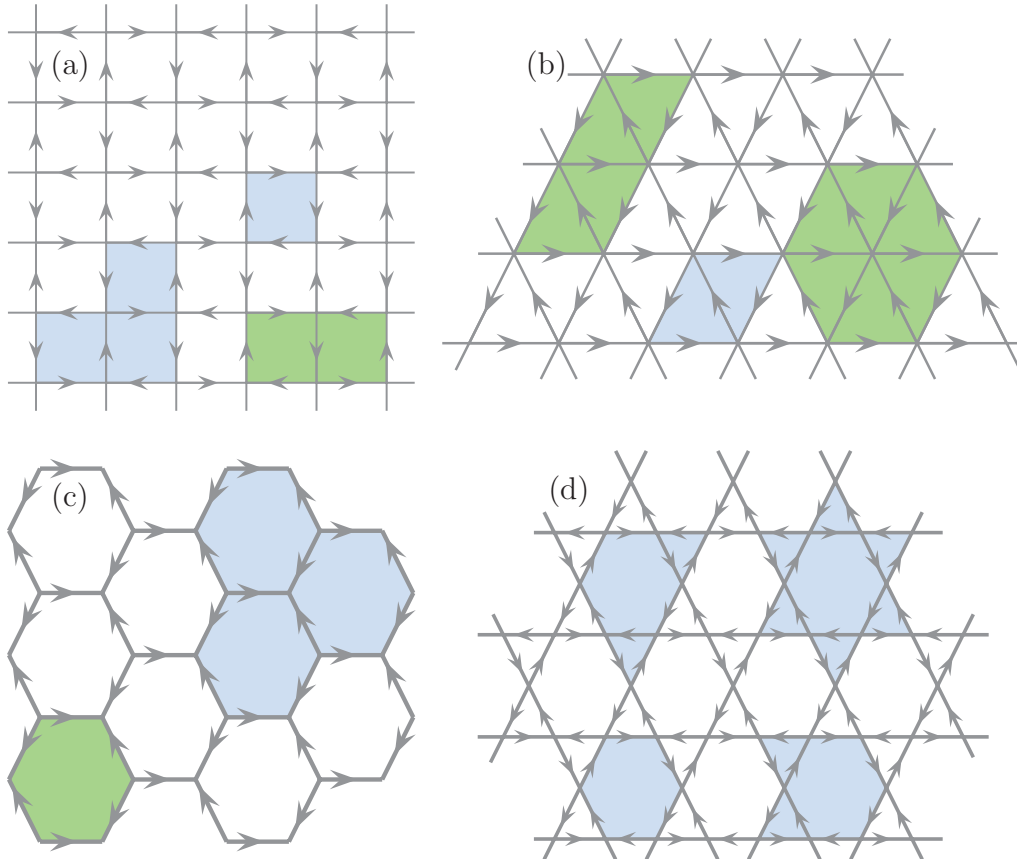


FIG. 4. (Color online) Bond prescriptions on the square (a), triangular (b), honeycomb (c), and kagome (d) lattices. Light-blue plaquettes have an even prescription while the green plaquette has an odd prescription.

Using the prescription $i \rightarrow j \rightarrow k$, the amplitude in the hopping term for the holes is the same if we use the fermionic or bosonic versions of the composite operators. Flipping two arrows we have the prescription $k \rightarrow j \rightarrow i$. It is a simple matter to see that with this prescription the hopping amplitude is also the same for the two cases.

Then, the hopping of the holes written in terms of bosonic and fermionic composite operators have the same amplitude t , provided that we use one of the two prescriptions satisfying that the intermediate site has one incoming and one outgoing arrow. If we take this $i \rightarrow j \rightarrow k$ prescription in all the sites of the lattice the arrows follow a sort of Kirchhoff’s first rule; see Figs. 4(a), 4(b), and 4(d). We will call this kind of prescription “zero-current” prescriptions. Of course it is only possible to satisfy this prescription in all the sites if the coordination number of the lattice is even. An example where this is not possible is the Honeycomb lattice (with $z = 3$). In this lattice it turns out that it is not possible to take a prescription with the same number of incoming and outgoing arrows in each site; see Fig. 4(c).

IV. QDM CLASSIFICATION FOR DIFFERENT LATTICES

A. On the choice of the bond orientation prescription

As we saw in the last section, in order to prove the equivalence between Hamiltonians built with bosonic and fermionic operators, one needs a bond orientation prescription for the fermionic case. Of course, this prescription is totally

arbitrary and before proceeding it is important to clarify the issue of a different choice of prescription. Let us imagine a generic lattice for which we have chosen two different prescriptions, A and B . To clarify the ideas, imagine that the orientation of all the bonds in prescription B are the same that in prescription A , except for one single bond, which is connecting points i and j . Then, starting from a bosonic Hamiltonian, by doing the transmutation, we end up with two different Hamiltonians H_A and H_B which have the same signs for all the flipping and hopping terms except for the ones that contain the bond ij . Let us illustrate this with the following example: consider the square lattice in which prescription A is the one given in Fig. 4. Then, imagine a prescription B where only the arrow between sites i and j is reversed, as shown in Fig. 5. Starting from the same bosonic Hamiltonian, after the statistical transmutation, we get the Hamiltonians H_A and H_B . What is the difference between H_A and H_B ? They have the same signs for all the flipping terms, except the the ones of plaquettes α and β , which are the only two containing this reversed bond. Also, all hopping terms are the same except those containing the link ij .

Although one could naively think that these two resulting Hamiltonians are not equivalent, in fact they are, as can be easily seen by performing the following gauge transformation:

$$\begin{aligned}
 b_{n,m}^\dagger &\rightarrow -b_{n,m}^\dagger \text{ if } n = i, m = j \text{ or } n = j, m = i, \\
 b_{n,m}^\dagger &\rightarrow b_{n,m}^\dagger \text{ else.}
 \end{aligned}$$

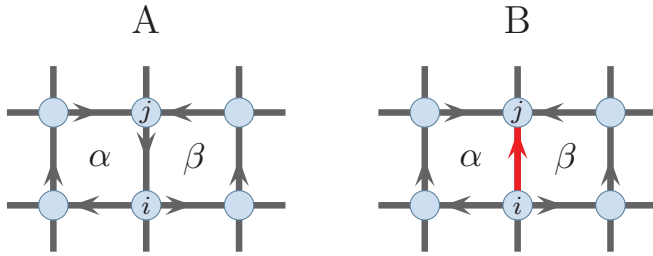


FIG. 5. (Color online) The change of prescription corresponding to reversing the orientation of one single bond (ij in the figure) corresponds to a gauge transformation where only configurations containing a dimer in the ij bond have their sign changed. This in turn has the effect of reversing the sign of the flipping and hopping terms containing the bond ij , as, for example, the flipping of plaquettes α and β .

Most generally, it is easy to convince oneself that different choices of prescriptions give rise to apparently different Hamiltonians which in fact are equivalent under a certain gauge transformation. We are now going to consider each lattice in detail and justify for each of them the choice of prescription we have made.

B. Square lattice

For the square lattice, we consider the prescription given in Fig. 4(a). Using this prescription, the hopping amplitude (t) remains equal for the bosonic and fermionic representation B and \tilde{B} . On the other hand, the kinetic amplitude corresponding to dimers (J_α) changes its sign if an even prescription is induced in the plaquette of length α . In Fig. 4 the plaquettes of lowest order are shown. Light-blue areas correspond to even prescriptions induced in the plaquettes while green areas correspond to odd prescriptions. The relative sign between the couplings in the fermionic and bosonic representations corresponding to the eight smallest plaquettes are presented in Table I.

TABLE I. Values of $\tilde{J}_\alpha/J_\alpha$ corresponding to the lowest orders of the resonant plaquettes on the square lattice.

N	Loop	$\frac{\tilde{J}/\tilde{t}}{J/t}$
2		-1
3		1
3		-1
4		-1
4		-1
4		1
5		1
5		1
5		1

TABLE II. Values of $\tilde{J}_\alpha/J_\alpha$ corresponding to the lowest orders of the resonant plaquettes on the triangular lattice.

N	Loop	$\frac{\tilde{J}/\tilde{t}}{J/t}$
2		-1
		-1
3		-1
		1
		1
		-1

C. Triangular lattice

For the triangular lattice, as in the square case, the coordination number is even and we can take a “zero-current” prescription as shown in Fig. 4(b). Then the hopping amplitudes for bosonic and fermionic holons have the same sign. Again, the change in the sign when we change from a bosonic representation of the holes to a fermionic one is determined by the parity of each flipping term. In Table II we show the results for flipping loops containing up to three dimers.

D. Honeycomb lattice

The case of the Honeycomb lattice is more subtle. The coordination number in this lattice is $z = 3$ and it is not possible to take a “zero-current” prescription. Therefore, it is not possible to find a prescription in which all the hopping terms would remain the same after the transmutation. We then use the prescription of Fig. 4(c) in which all the hopping amplitudes for the holes change the sign when we change to the fermionic representation of the operators ($\tilde{t}_n = -t_n$).

The relative signs between the ratios \tilde{J}/\tilde{t} and J/t are presented in Table III for plaquettes of three, five, and six dimers.

E. Kagome lattice

For the kagome lattice, we have chosen the prescription depicted in Fig. 4(d). All the possible allowed flipping terms

TABLE III. Values of $\tilde{J}_\alpha/J_\alpha$ corresponding to the lowest orders of the resonant plaquettes on the honeycomb lattice.

N	Loop	$\frac{\tilde{J}/\tilde{t}}{J/t}$
3		-1
5		-1
6		1

up to 12 bonds are depicted in Table VI of the Appendix. Is it interesting to note that these loops are all, without exception, even. This feature is not specific to loops of short lengths and one can convince oneself that all allowed flipping loops of arbitrary length are even. Moreover, our prescription choice is such that the hopping terms within one triangle remain invariant under the statistical transmutation. From this, one can conclude that a Hamiltonian with flipping terms $\{J_l\}$ and bosonic holes is equivalent to a Hamiltonian with fermionic holes and with the signs of all flipping terms reversed $\{-J_l\}$.

One last remark one can make about the kagome lattice relies on its intrinsic flexibility. Take any triangle of it and change the orientation of the three bonds belonging to that triangle only. It is easy to see that with the new prescription all the hopping terms, including those belonging to the chosen triangle, do not change signs. However, the flipping terms containing one (and only one) bond belonging to that triangle will change their signs, i.e., these flipping terms in the transmuted Hamiltonian have the same sign as in the bosonic model. What this means is that, in contrast to the other lattice studied here, it is possible on the kagome lattice to build gauge transformations which leave invariant the sign of all hopping amplitudes while changing the sign of “some” flipping terms (even locally).

F. Example of application of the “statistical transmutation” symmetry

To illustrate the power and extent of our results, we concentrate on a couple of concrete examples taken on the square and triangular lattices, respectively. Let us consider the QDM defined on the square lattice with only two and three dimer flipping terms. These terms correspond to the first and second row of Table I. Its sibling model can be defined on the triangular lattice by just considering the terms with $N = 2$ and only the second of the terms with $N = 3$ in Table II. In principle we would have 16 inequivalent Hamiltonians in each case. However, our statistical transmutation result tells us that the number of inequivalent Hamiltonians is smaller. Indeed, we find only eight inequivalent Hamiltonians for the case of the triangular lattice, which we dubbed I_σ , II_σ , III_σ , and IV_σ , where $\sigma = \pm$ corresponds to the sign of the hopping term. From these eight classes only four classes are inequivalent for the case of the square lattice. The smaller number of equivalence classes in the latter case is due to the equivalence $t \leftrightarrow -t$ which is valid for the square lattice but not for the triangular lattice.¹⁸ The result is summarized in Table IV.

G. Transformation of assisted terms

When a QDM is regarded as a low-energy effective model of frustrated antiferromagnets, it is important to see if other kinds of term, apart from those already mentioned here, arise in the effective QDM Hamiltonians. Examples of derivation of the QDM Hamiltonian arising from microscopic Heisenberg models can be found in Ref. 9 for the square lattice with second- and third-neighbor couplings and in Ref. 10 for the kagome lattice. In these QDMs appears a third kind of diagonal or off-diagonal terms, which are dubbed assisted terms. Let us now discuss these assisted terms in our framework. An example of such terms is given in the last row of Table I

TABLE IV. Classification for the doped QDM with resonant plaquettes of length 4 and 6. For the square lattice the families I_+ and I_- are equivalent (*idem* families II, III, and IV). For the triangular lattice J_4 corresponds to the three resonant plaquettes corresponding to $N = 2$ in Table II whereas J_6 corresponds to the second row of $N = 3$ in the same table. The last two columns show the references where such models have been studied (for $J_6 = 0$) on square (\square) and triangular (\triangle) lattices.

Statistics	J_4	J_6	t	Family	Refs. (\square)	Refs. (\triangle)
Bosons	+	+	+	I_+	23, 24, 25, 26	18, 24, 26
Bosons	+	+	-	I_-	23, 25	18
Bosons	+	-	+	II_+		
Bosons	+	-	-	II_-		
Bosons	-	+	+	III_+	23	18
Bosons	-	+	-	III_-	23	18
Bosons	-	-	+	IV_+		
Bosons	-	-	-	IV_-		
Fermions	+	+	+	III_+	23	18
Fermions	+	+	-	III_-	23	18
Fermions	+	-	+	IV_+		
Fermions	+	-	-	IV_-		
Fermions	-	+	+	I_+	23	18
Fermions	-	+	-	I_-	23	18
Fermions	-	-	+	II_+		
Fermions	-	-	-	II_-		

in Ref. 9. They consist of diagonal or off-diagonal terms of the kind of the H_V and H_J in Hamiltonian (1) but subject to the condition that a third dimer is sitting in another given neighboring bond. Such kind of term can be written as, for example,

$$[b_{i,j}^\dagger b_{k,l}^\dagger b_{j,k} b_{l,i} + \text{H.c.}] [b_{m,n}^\dagger b_{m,n}], \quad (34)$$

whose effect is to flip two parallel dimers sitting in the plaquette i, j, k, l provided that there is one dimer sitting in the plaquette m, n . By extending the arguments developed above, one can show that under the statistical transmutation, this kind of term transforms in the very same way as the corresponding nonassisted term. For example, the term written above would transform in the same way as the term

$$b_{i,j}^\dagger b_{k,l}^\dagger b_{j,k} b_{l,i} + \text{H.c.} \quad (35)$$

This is simply due to the fact that assisted terms can be written as the product of traditional diagonal or off-diagonal operators which we know already how they transform and projectors which are written in terms of dimer density operators which are invariant under the statistical transmutation.

V. NUMERICAL INVESTIGATION OF QDMs ON THE TRIANGULAR LATTICE

A. Summary of phase diagrams in Ref. 18

We now complement the analytical exact results with a numerical study. In our previous work,¹⁸ we concentrated on the triangular lattice because it is the best laboratory for using our analytic results on the statistical transmutation symmetry and for investigating doped dimer liquid phases. Here we shall push these studies further but we start with a brief summary

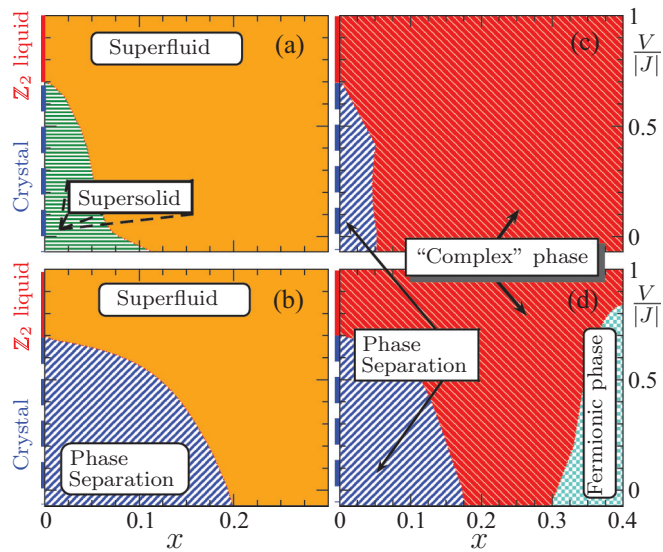


FIG. 6. (Color online) Qualitative phase diagrams of four inequivalent doped QDM's on the triangular lattice versus doping (x) and $V/|J|$ for fixed $t/J = 0.5$, from Ref. 18. All the models have only flipping terms corresponding to $N = 2$ in Table II. Case (a) corresponds to positive J and t and bosonic holes, (b) is obtained from (a) by changing the sign of the hopping term t , (c) is obtained from (a) by changing the bosons to fermions, and (d) is obtained from (b) by changing the bosons to fermions.

of the results obtained in Ref. 18. Considering only flipping terms $J = J_4$ involving the shortest loops corresponding to $N = 2$ in Table II a topological (\mathbb{Z}_2) liquid can be stabilized at zero doping^{5,27} (the sign of J is irrelevant for $x = 0$). At finite doping, four nonequivalent families of Hamiltonians can be constructed depending on the signs of t and J . Note that changing the bare statistics of the holons does not introduce a new class of Hamiltonian since this is equivalent to change the sign of J as seen in the previous sections. In other words, one can equivalently choose to work in the bosonic or fermionic representations. In contrast, the actual statistics of the elementary excitations has to be studied numerically. One can use, e.g., the method developed in Ref. 23 which consists of investigating the node content of the wave functions.

The phase diagrams of the four families of models obtained in Ref. 18 are reproduced in Fig. 6 for convenience. At zero doping (where the four models merge into the same $x = 0$ limit) there are two (insulating) phases, (i) a six-site cell valence-bond crystal (VBC) for $0 \leq V/|J| \leq 0.7$ and (ii) a topological \mathbb{Z}_2 dimer-liquid above. At finite doping, family (a) in Fig. 6 is the only unfrustrated case and was studied using the Green's function Monte Carlo (GFMC) methods in Ref. 24. In this model bare holons are bosonic and remain representative of the physical excitations in the entire region of the phase diagram, as happens also in the Perron-Frobenius square lattice version, studied in Ref. 23. The situation is even more interesting when J is changed into $-J$, or equivalently, bosons are changed into fermions [families (c) and (d) in Fig. 6]. Finally, changing the signs of both J and t of the unfrustrated model (a) leads to the complex case (d). Note that the PS regions are further increased at $V < 0$ so we restrict here only to $V > 0$.

When J becomes comparable to the holon average kinetic energy (of order xt) holons may be macroscopically expelled from the dimer fluctuating background, in order to minimize the dimer resonance energy. The question of *phase separation* (PS), i.e., the possibility for the system to spontaneously undergo a macroscopic segregation into two phases with different hole concentrations, was considered in Ref. 18. In order to perform a Maxwell construction one can define $s(x) = [e(x) - e(0)]/x$, where $e(x)$ is the energy per site at doping $x = n_h/N$ (n_h is the number of holons in the system and N the number of sites). In the case of PS, the energy presents a change of curvature at a critical doping x_c corresponding to the minimum of $s(x)$ as a function of x . The fact that the local curvature of $e(x)$ at $x = 0$ is negative then implies that the two separated phases will have $x = x_c$ and $x = 0$ (the undoped insulator) hole concentrations. This study revealed that all frustrated [(b)–(d)] models show a finite PS region [shown in blue in Figs. 6(b)–6(d)] at low doping. The extension vs $V/|J|$ of this region seems to coincide with the $x = 0$ VBC. In contrast, the nonfrustrated (a) model does not show phase separation at $V > 0$ (as already seen in GFMC simulations) but, rather, shows a homogeneous region at finite doping where VBC order survives. Because of the coexisting nonzero superfluid order [U(1) symmetry breaking, see below], this phase can be viewed as a “supersolid” (SS). Here supersolidity involves *hole pairing* in the vicinity of a (insulating) VBC phase (and in the absence of PS), as also found in the *frustrated* doped QDM on the square lattice²³ or in doped frustrated spin-1/2 quantum magnets.²⁸

Another important quantity used in Ref. 18 is the sign operator defined in Ref. 23 which provides a quantitative analysis of the nodal structure of the wave function and hence gives insights about the statistical nature of the holons, i.e., whether they truly behave as bosons or fermions. Such an analysis clearly showed that the GS of models (a) and (b) have the same nodal structure as a superfluid. For models (c) and (d), we dubbed a “complex phase” as the statistics of dressed excitations does not correspond solely to bosons or fermions. Family (d) also shows, in addition, an interesting fermion reconstruction at large doping, which we call the “fermionic phase”. In this work we have extended the study of the nodal structure for larger values of the doping than the ones of Fig. 6. Our results clearly show that for $x \gtrsim 0.6$ the elementary excitation behaves as bosons for the four models. This means in particular that in model (d) a dynamical statistical transmutation took place in which each Fermion bound to a vison in order to form a boson. As we show below, this result has important consequences in the nature of the superfluid phases that we find for those values of the doping.

Finally, an Aharonov-Bohm flux can be inserted in one of the hole of the torus, as done in Ref. 26 for the doped QDM on the square lattice. A superfluid is characterized by well-defined minima in the ground-state energy separated by a finite barrier in the thermodynamic limit. *Contrario*, in a typical signature of (weakly interacting) fermions, a flat energy profile is expected even on such a small cluster.²⁹ Here, it was reported in Ref. 18 that the ground-state energy has well-defined minima quantized at half a flux quantum for all family of models at $x \sim 0.25$. This might appear as an evidence for condensation of charge- $2e$ particles. However,

as already discussed in Sec. III A, the $\pi/(2e)$ -flux periodicity is a generic feature of doped QDMs and does not rule out the possibility of condensation of deconfined charge- e holons. Next, we will characterize more thoroughly the nature of the superfluid phases, by introducing a gauge-invariant holon Green's function to distinguish the charge- e condensation from the usual charge- $2e$ condensation.

B. New correlations to explore the nature of the superfluid phases

In order to understand the nature of the superfluid phases the effective charge of the quasiparticles that condensate have to be determined—either charge- e or charge- $2e$ quasiparticles. This is related to the mechanism that leads to the spontaneous breaking of the U(1) symmetry expected in a superfluid. As a first attempt, one could naively use the correlation function $\langle a_i^\dagger a_j \rangle$, but it is not compatible with the constraint (8). In other words, it is not gauge invariant and thus this correlation function is zero. To satisfy the constraint, or equivalently the gauge invariance, we need to write correlations in terms of operators B . As the hopping of holes can be written in terms of operators B we can move one of the holes between two distant sites by applying a string of $B^\dagger B$'s.

1. Gauge invariant holon Green's function

In the subspace where the constraint is satisfied pairs of holons operators $a_i a_i^\dagger$ acting on sites without holes are equal to the identity. Then the holon Green's function we want to calculate is given by

$$G_{i,j}^{(b)} = \sum_n \langle a_i^\dagger \mathcal{S}_{j,i}^{(n)} a_j \rangle, \quad (36)$$

where $\mathcal{S}_{j,i}^{(n)} = b_{j,n_1}^\dagger b_{n_1,n_2} b_{n_2,n_3}^\dagger b_{n_3,n_4} \dots b_{n_{N-1},n_N}^\dagger b_{n_N,i}$ is a string operator between the sites i and j following the path n . The label (b) indicates that the holes are taken as bosons. Similarly, the fermionic version of the Green's function is written as

$$G_{i,j}^{(f)} = \sum_n \langle f_i^\dagger \mathcal{S}_{j,i}^{(n)} f_j \rangle. \quad (37)$$

Note that, since there are many ways of moving a hole between two sites, the gauge invariance alone does not uniquely determine the definition of the holon Green's function. Here we adopt the definition with a sum over all possible strings (labeled by n) connecting the two sites i and j , with the same coefficient. This definition appears most natural to us, as well as in numerical implementation. We expect that other definitions with some restrictions on strings would also work as an order parameter. However, the present definition looks advantageous in numerical calculations, since it can efficiently detect the holon condensation with the summation over all possible strings. Notice that, because of the constraint on the dimers, the paths are necessary self-avoiding.

Using a complete basis of dimer/hole configurations the correlations can be rewritten as

$$G_{i,j}^{(b)} = \sum_n \sum_{\alpha,\beta} \langle \psi | \alpha \rangle \langle \beta | \psi \rangle \langle \alpha | a_i^\dagger \mathcal{S}_{j,i}^{(n)} a_j | \beta \rangle, \quad (38)$$

$$G_{i,j}^{(f)} = \sum_n \sum_{\alpha,\beta} \langle \psi | \alpha \rangle \langle \beta | \psi \rangle \langle \alpha | f_i^\dagger \mathcal{S}_{j,i}^{(n)} f_j | \beta \rangle. \quad (39)$$

The holon Green's function can be also written in terms of the composite operators only,

$$G_{i,j}^{(b)} = \sum_{\{n\}} \langle B_{N-1,N}^\dagger B_{N,i} \dots B_{2,3}^\dagger B_{3,4} B_{1,j}^\dagger B_{1,2} \rangle, \quad (40)$$

$$G_{i,j}^{(f)} = \sum_{\{n\}} \langle \tilde{B}_{N-1,N}^\dagger \tilde{B}_{N,i} \dots \tilde{B}_{2,3}^\dagger \tilde{B}_{3,4} \tilde{B}_{1,j}^\dagger \tilde{B}_{1,2} \rangle, \quad (41)$$

where the sum is over all possible paths between sites i and j . One can use this representation to show that the two correlations are in fact equal, up to an irrelevant sign. In other words, we have

$$G_{i,j}^{(b)} = \pm G_{i,j}^{(f)}, \quad (42)$$

where the relative sign depends only on the *relative* distance between i and j . Off-diagonal long-range order of $G_{i,j}$ is a fingerprint of the spontaneous breaking of the U(1) gauge symmetry (associated to charge conservation). It also implies that the condensing quasiparticles have charge e . It is also interesting to observe that at large doping, this Green's function must necessarily have an exponential decay (see below). Indeed, the Green's function for being nonzero needs at least one path in which dimers are present all along it (the string). For a large concentration of holes $x \rightarrow 1$ it is more and more unlikely to find a path with dimers on it so that the Green's function $G_{i,j}$ should roughly decay as $(1-x)^L$ where L is the distance between points i and j .

Another observable which can detect the charge- e condensation is

$$F_{i,j} = \langle a_i^\dagger \mathcal{S}_{j,i}^{(n)} a_j \rangle, \quad (43)$$

when a symmetry-breaking ground state (when it occurs) formed by superposition over different dimer-number sectors is used. Roughly speaking, this corresponds to the square of the expectation value of a single hole creation operator $\langle a^\dagger \rangle$ in the ground state, defined in a gauge-invariant manner. Such an expression is however less convenient to compute numerically in finite-size systems and will not be used.

The scenario of Bose condensation of polarized spinons (the holons in our current formulation) under an applied magnetic field advocated in Ref. 24 implicitly implies long-range order of G_{ij} . We wish here to substantiate such a scenario by an explicit computation of this correlation function.

2. Hole pair correlations

If $G_{i,j}$ is short ranged, there is no condensation of charge- e holons. However, spontaneous U(1) symmetry breaking and, hence, superfluidity can still occur provided the (hole) pair-pair correlation,

$$P_{i,j,k,l} = \langle B_{i,j} B_{k,l}^\dagger \rangle, \quad (44)$$

exhibits long-range order (LRO). The pair-pair operator is connected to the square of the single holon effective hopping

TABLE V. Classification of the possible phases, including various superfluid (SF) phases, that may occur in doped QDM's on the triangular lattice. Such phases can be distinguished from the sign of the compressibility κ , the long-distance properties ("SR" means short-range, "LR" means long-range) of various correlations, or the effective charge deduced from periodicity of the GS energy versus a magnetic flux inserted through a torus. sgn_B and sgn_F were defined in Ref. 23 to analyze the node content of the GS wave function.

Observables→ Phases↓	κ	$\langle b_{i,j}^\dagger b_{i,j} b_{k,l}^\dagger b_{k,l} \rangle$	$\langle a_k^\dagger a_l^\dagger a_i a_j \rangle$	$\langle a_i^\dagger S_{i,j} a_j \rangle$	sgn_B	sgn_F	Flux periodicity
PS	<0						
VBC	>0	LR	SR	SR			$2e$
SS	>0	LR	LR	SR	1	0	$2e$
$2e$ -SF	>0	SR	LR	SR	$0 < \text{sgn}_B < 1$	$0 < \text{sgn}_F < 1$	$2e$
e -SF	>0	SR	LR (weak)	LR	1	0	$2e$
Bose liquid	>0	SR	SR	SR	1	0	$2e$
Fermi liquid	>0	SR	SR	SR	0	1	$2e$
"Complex" phase	>0	SR	SR	SR	$0 < \text{sgn}_B < 1$	$0 < \text{sgn}_F < 1$	$2e$

operator in a complicated manner. Namely,

$$\begin{aligned}
 & \left(a_i^\dagger \sum_n \mathcal{S}_{k,i}^{(n)} a_k \right) \left(a_j^\dagger \sum_{n'} \mathcal{S}_{l,j}^{(n')} a_l \right) \\
 & + \left(a_i^\dagger \sum_n \mathcal{S}_{l,i}^{(n)} a_l \right) \left(a_j^\dagger \sum_{n'} \mathcal{S}_{k,j}^{(n')} a_k \right) \\
 & = B_{i,j} B_{k,l}^\dagger + \{\text{loop terms}\}, \quad (45)
 \end{aligned}$$

where the first part of the right-hand side is obtained from a "closure relation" involving all pairs of "retraceable" strings $n' = \bar{n}$, i.e.,

$$\sum_n (\mathcal{S}_{k,i}^{(n)} \mathcal{S}_{l,j}^{(\bar{n})} + \mathcal{S}_{l,i}^{(n)} \mathcal{S}_{k,j}^{(\bar{n})}) = b_{ij} b_{kl}^\dagger, \quad (46)$$

and the rest corresponds to pair hopping dressed with extra loop fluctuations. The proof for Eq. (46) is not straightforward but the reader may be easily convinced of this result by drawing the paths for some examples. This suggests that it is physically meaningful to write the pair correlations as

$$P_{ijkl} = G_{ik} G_{jl} + G_{il} G_{jk}, + P_{ijkl}^c, \quad (47)$$

where the first two terms can be viewed as the "mean-field" contribution and P_{ijkl}^c stands for the "connected" part in which we remove all the processes involving compositions of single holon hoppings. In particular, both sides scale like x^2 or $(1-x)^2$, respectively, in the limit $x \rightarrow 0$ or $x \rightarrow 1$. Therefore it is convenient to normalize P_{ijkl} by $x^2(1-x)^2$ and G_{ij} by $x(1-x)$. Equation (47) shows that LRO in the holon Green's function $G_{ik} \rightarrow G_\infty$, characteristic of the charge- e superfluid, will inevitably induce LRO in the pair-pair correlation, $P \sim G_\infty^2$. In contrast, the conventional, charge- $2e$ superfluid is defined by LRO in the connected part *together with the short-ranged holon Green's function*.

3. Dimer-dimer correlations

We finish by recalling that the dimer-dimer correlations are expressed in terms of the dimer number operators $b_{i,j}^\dagger b_{i,j}$ as

$$N_{i,j,k,l} = \langle b_{i,j}^\dagger b_{i,j} b_{k,l}^\dagger b_{k,l} \rangle, \quad (48)$$

where sites i and j on one hand, and k and l on the other hand, are nearest-neighbor sites. Long-range order in this correlation

function is characteristic of VBC order. The wave vector at which the associated structure factor diverges defines the VBC wave vector.

In principle, one can use the new correlations $G_{i,j}$ and $P_{i,j,k,l}$ to refine the previous phase diagrams ($N_{i,j,k,l}$ was used in previous work to determine the VBC and SS regions). To ease the analysis of the numerical results of the doped QDM's, a classification of the various possible phases based on simple considerations is provided in Table V.

We note that there is no phase where there is a charge- e condensation simultaneously with a dimer long-range order ("LR" for both $\langle b_{i,j}^\dagger b_{i,j} b_{k,l}^\dagger b_{k,l} \rangle$ and $\langle a_i^\dagger S_{i,j} a_j \rangle$.) This is because existence of the dimer long-range order leads to confinement of holons.

C. Numerical results

In Fig. 8 are displayed both the holon Green's functions [Eqs. (36) and (37)] and the *square root* of the pair-pair correlations [Eq. (44)] computed by numerical exact diagonalization on a 16-site triangular cluster, varying the hole density from $x = 0.125$ (low hole concentration) to $x = 0.75$ (low dimer concentration), from top to bottom. For convenience, both

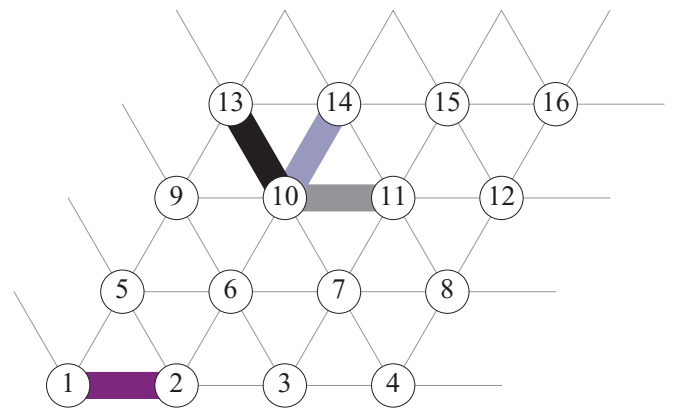


FIG. 7. (Color online) Sixteen site cluster: labeling of the sites (numbered circles) and reference bond (purple bond) used respectively in the definition of Green's functions and the pair correlations. The bonds are labeled according to one of the sites connected to them and by a direction, as shown in the example (here site 10).

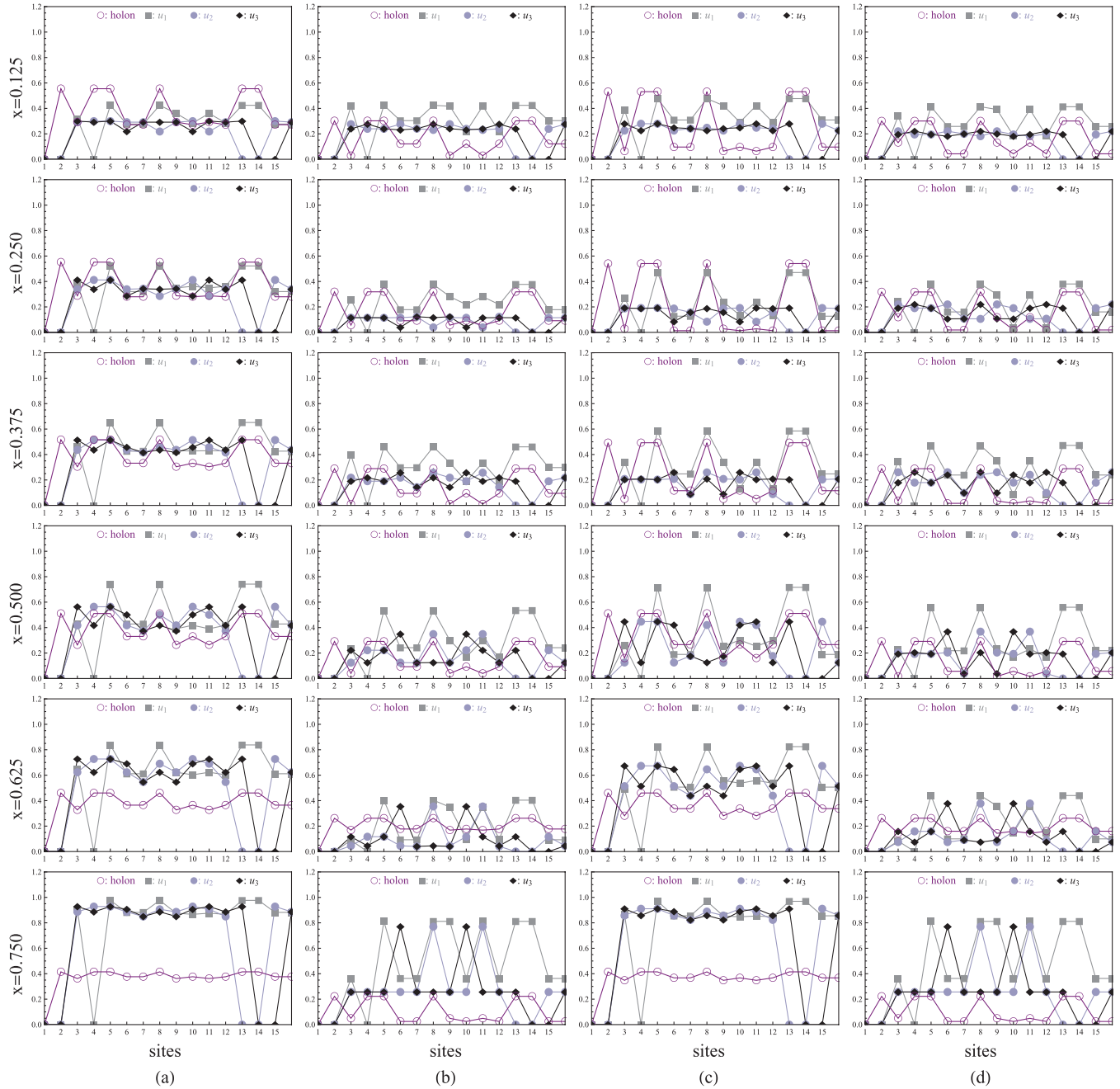


FIG. 8. (Color online) Holon Green’s function (open circles) and *square root* of the absolute value of the pair-pair correlations (filled symbols) for parameters $V = 0.3$, $|J| = 1.0$, and $|t| = 0.5$, at various densities ranging from $x = 0.125$ to $x = 0.75$ (2 to 12 holons on 16 sites) and for the four classes (a)–(d) of models defined in the caption of Fig. 6. The pair-pair correlation $P_{i,j,k,l}$ is defined by a reference bond orientation $\vec{r}_j - \vec{r}_i = \vec{u}_\alpha$ and the orientation of the final bond $\vec{r}_l - \vec{r}_k = \vec{u}_\beta$. In our case, we chose $\vec{u}_\alpha = \vec{u}_1$ and we consider three cases for \vec{u}_β : \vec{u}_1 (filled squares), \vec{u}_2 (filled circles), and \vec{u}_3 (filled diamonds)—see Fig. 7.

the Green’s functions and the *square root* of the pair-pair correlations are normalized by $x(1 - x)$ to be able to use the same scale for all densities. The four Hamiltonian classes defined previously (see, e.g., the caption of Fig. 6) are depicted in parallel panels (a)–(d), respectively. For all of them, we chose the parameters $V = 0.3$, $|J| = 1.0$, and $|t| = 0.5$ for which, at holon density $x = 0.25$, the system is either in a superfluid phase [Figs. 6(a) and 6(b)] or in the “complex” phase [Figs. 6(c) and 6(d)], depending on the QDM class.

Let us first discuss the data at the lowest hole densities $x \leq 0.5$. As one can see, only model (a) presents a large amplitude of the holon Green’s function away from the reference site (the largest disk) and its six neighbors. While a definite conclusion cannot be drawn from such small system, a direct comparison between model (a) and the three others reveals a clear change of behavior. Indeed, for models (b)–(d), the holon Green’s function decreases at the largest available distances to significantly smaller values, except

maybe for model (c) around $x \sim 0.5$. On the other hand, the pair-pair correlations, for which the reference link is in the \vec{u}_1 direction, show convergence with bond separation to a uniform value for model (a) in all relative directions of the two bonds, while these correlations are strongly reduced for directions differing from that of the reference bond in the other models. Hence our data are clearly compatible with model (a) being in the charge- e superfluid phase described in Table V, unambiguously revealing strong signals simultaneously in the holon Green's function and the pair-pair correlation. Note that we also checked that the dimer-dimer correlations (not presented here) remain SR in model (a) hence reinforcing the previous claim. The behavior of the other models at low to moderate doping is less clear, with quite smaller amplitudes of G_{ij} and P_{ijkl} at the largest available distances. We can, however, recognize a possible $2e$ -superfluid phase in model (c) after the phase separation zone and up to values of $x \simeq 0.2$.

While increasing holon density, from $x = 0.5$ to $x = 0.75$, we observe that the data for the bosonic and fermionic models become identical, both for $t > 0$ or $t < 0$. This can be understood by the fact that the (bosonic) dimers become then the relevant entities instead of the holes. This implies, in particular, that statistical transmutation or pairing must occur for increasing x for the models where fermionic statistics is expected at small x [models (c) and (d)]. This is indeed confirmed by the analysis of the nodal structure of the wave functions that we performed for $x = 0.625$. In this sense the complex phase found in model (c) is probably the region in which fermions bound to visons and transmute, in order to resemble the bosonic excitations of model (a). Note also that charge- e superfluidity seems to occur at $x = 0.625$ in models (a) and (c) (which seems equivalent for this doping).

However, at larger x corresponding to a dilute gas of dimers one expects to eventually recover a charge $2e$ superfluid via a continuous (second order) or discontinuous (first order) phase transition. This seems to occur already for $x = 0.75$ for models (b) and (d), for which only the pair-pair correlations are sizable at the largest distances. We have checked that for a lower dimer density of $1 - x \sim 0.1$ G_{ij} is short range for *all* models as reported in Fig. 9. In the limit of a very dilute gas of dimers, pairing between dimers because of the kinetic term J is also a possibility. This could result in either phase separation or in a homogeneous phase in which both G_{ij} and P_{ijkl} are short ranged but which is nevertheless superfluid, of coherent dimer pairs of charge $4e$. We have checked that there is no phase separation in any of the four models at those large values of x . We have also looked at the energy difference between two and one dimers and found that pairing is indeed favored in models (b) and (d) which may explain the drop of the P_{ijkl} in Fig. 9 for $x \gtrsim 0.9$.

Based on Figs. 6, 8, and 9, we have extracted the qualitative phase diagrams for the four models at fixed $V/|J| = 0.3$ and $t/|J| = 0.5$ as a function of doping x . They are depicted in Fig. 10. Charge- e superfluidity seems to occur in all models, with the largest occurrence in model (a). For intermediate doping, models (b) and (d) seem to present short-range correlations for both one- and two-particle Green's functions. This behavior suggests an uncondensed phase which in the

case of model (d) would correspond to a Fermi-liquid state. Since elementary excitations in model (b) are bosonic the presence of an uncondensed phase points toward an exotic Bose-liquid state, although this statement should require a more detailed study (using clusters of a much bigger size) which is beyond the scope of the present paper. For large x , all models exhibit a charge- $2e$ superfluid phase as expected, followed by a charge- $4e$ superfluid phase in models (b) and (d) due to dimer pairing.

VI. CONNECTION TO BOSE-HUBBARD MODELS

We finish this work by discussing the connection to Bose-Hubbard-like models which do not contain *a priori* the ice-rule constraint. However, the physics of the doped QDM can emerge naturally when some form of large repulsion between the itinerant bosons is considered, hence providing emergence of fractionalized excitations.³⁰

In Ref. 30 was introduced a simple model of hard-core bosons hopping (t) on a kagome lattice with a boson repulsion V_\square favoring the smallest number of bosons in each hexagon,

$$H = -t \sum_{(i,j)} (d_i^\dagger d_j + d_i d_j^\dagger) + V_\square \sum_{\square} (n_\square)^2, \quad (49)$$

where d_i^\dagger creates a boson on site i and $n_\square = \sum_{i=1}^6 d_i^\dagger d_i$ is the number of bosons in a hexagonal plaquette. When the boson density is $\rho = 1/2$ a large V_\square/t stabilizes an insulating phase whose quantum dynamics is described by a generalized QDM on the triangular lattice with exactly three dimers per site. The insulating phase is a \mathbb{Z}_2 topological liquid. When $t < 0$ the model is not frustrated and can be studied with QMC: the superfluid-insulator transition was argued to be a novel nonconventional *fractional critical point*.³⁰

To make the connection with some of our doped QDM's we shall assume here that the microscopic d bosons have charge $-2e$ and their density is set to $\rho = \frac{1}{6}(1 - x/2)$, $x \ll 1$. In that case, as shown in Fig. 11, for $V_\square/t \rightarrow \infty$ the lowest-energy configuration space ($E = NV_\square/3$) is given by all hard-core dimer coverings on an effective triangular lattice, where each d boson has been replaced by a dimer connecting two sites of the triangular lattice. Such configurations respect a local *ice-rule* constraint with one, and only one, boson per hexagon. When $x = 0$, moving a single d boson violates this ice rule so one has to move at least two simultaneously. This process of amplitude $J = t^2/V_\square$ corresponds exactly to a dimer flip on a lozenge, identical to the one of the QDM. Strictly speaking this mapping onto the QDM does not involve any dimer-dimer repulsion V . However, one can add a small third-nearest-neighbor density-density repulsion $V_{dd} \ll V_\square$ between the d bosons located on different hexagons. In the mapping for large V_\square/t , this interaction translates directly into the dimer-dimer repulsion $V = V_{dd}$. Thus, by tuning V_{dd} in the Bose-Hubbard model, the topological \mathbb{Z}_2 (insulating) liquid can be stabilized.

When $x \neq 0$ an empty site on the original kagome lattice corresponds to two "defect" hexagons carrying an overall charge $2e$ with respect to the insulating ground state. It is easy to see (Fig. 11) that each "defect" hexagon can move independently on the effective triangular lattice by simple processes that involve a single d -boson hopping. Therefore,

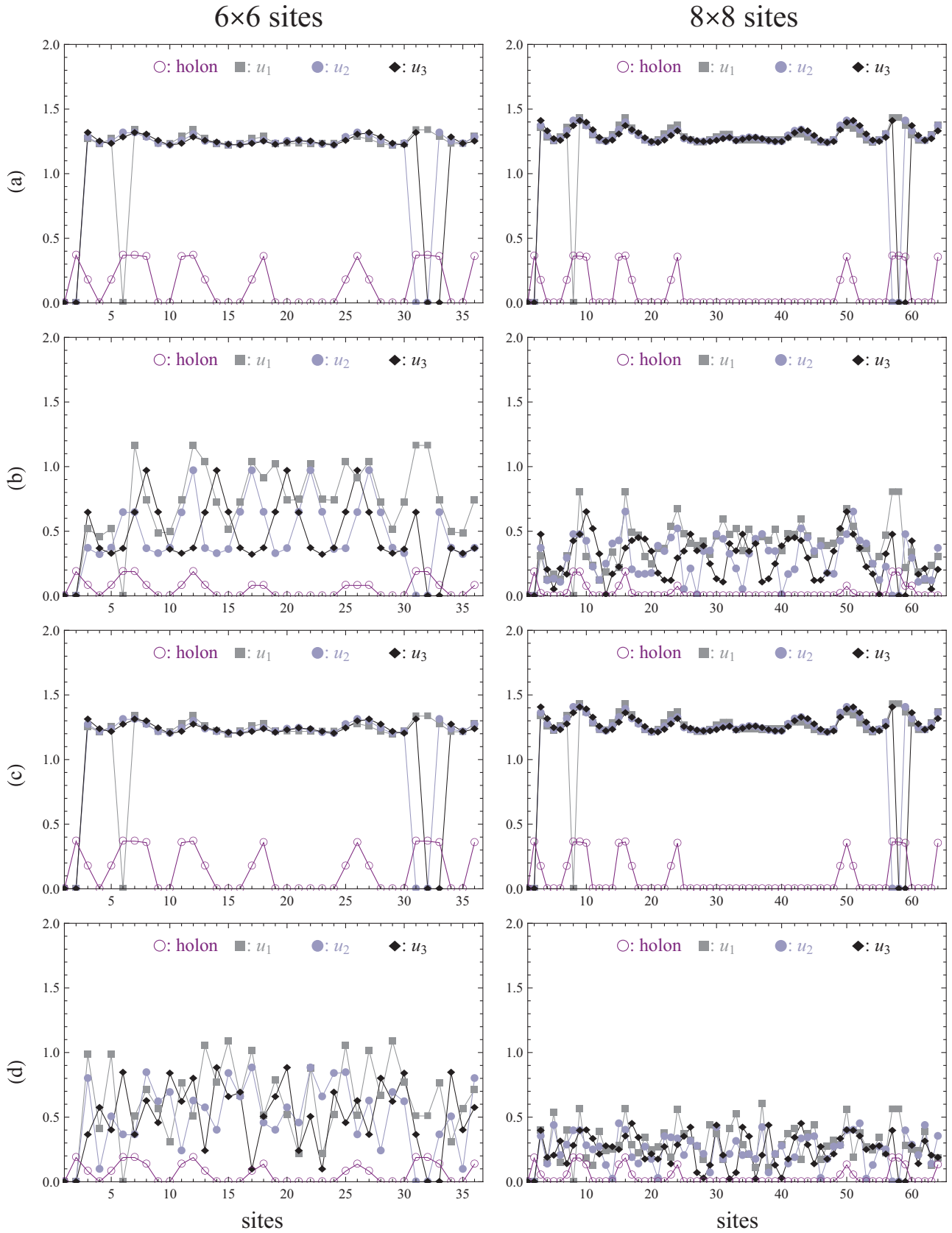


FIG. 9. (Color online) Holon Green's function (open circles) and *square root* of the absolute value of the pair-pair correlations (filled symbols) for parameters $V = 0.3$, $|J| = 1.0$, and $|t| = 0.5$, at a low dimer density $1 - x \simeq 0.1$ for the four classes (a)–(d) of models defined in the caption of Fig. 6. Left: two dimers on a 36-site cluster ($x \sim 0.89$). Right: three dimers on a 64-site cluster ($x \sim 0.91$).

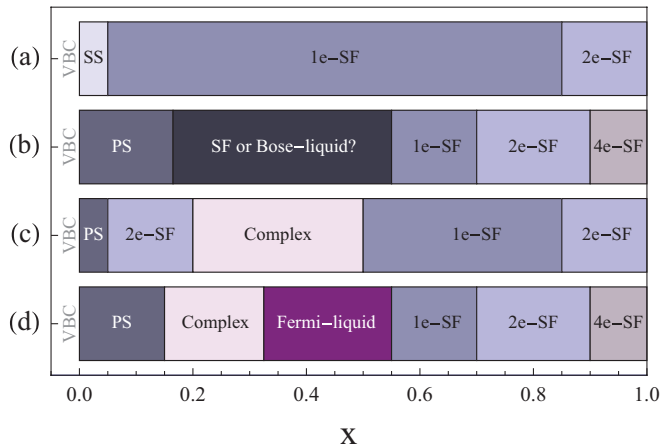


FIG. 10. (Color online) Phase diagrams of the four models (a)–(d) at $V/|J| = 0.3$ and $t/|J| = 0.5$ derived from Figs. 6 and 8. All have both the charge- e superfluid (e -SF) and charge- $2e$ superfluid ($2e$ -SF) phases at different doping depending on the model.

each “defect” can be considered as an effective charge- e hole on the triangular lattice. The amplitude t of the hole hopping is the same as the one of the microscopic d -boson Hubbard model. When a d boson of charge $-2e$ hops by a lattice spacing a , the effective hole of charge e hops by a distance $2a$ so that the charge center of mass is conserved. Note also that the hole density in the effective QDM is x .

The mapping to the doped QDM on the triangular lattice is therefore complete. However, it is important to notice that $J = t^2/V_{\square} > 0$ (for real t) so that only QDM (a) and (b) can be realized with HCB depending on the sign of t . Introducing imaginary hopping $t = i\tau$ on the kagome lattice equivalent to putting $U(1)$ fluxes through the triangles leads

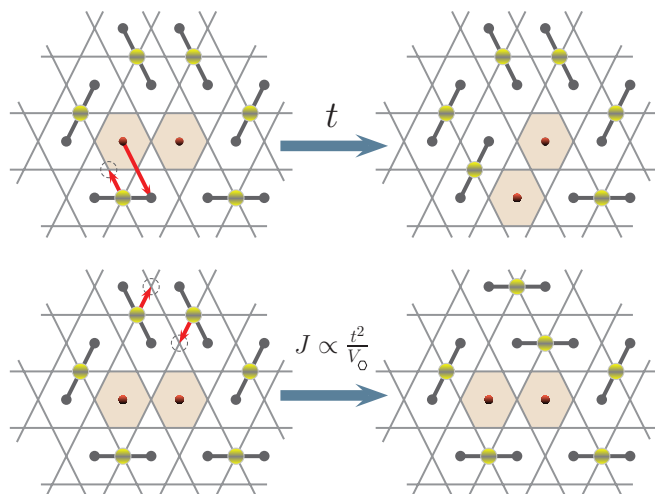


FIG. 11. (Color online) Hard-core bosons on the kagome lattice. Covering the lattice with one, and only one, boson per hexagonal plaquette (ice-rule constraint), we can identify distribution of bosons with a dimer hard-core covering on the triangular lattice. Removing a boson of charge $2e$ creates two defect hexagons (shaded). Each defect (hole) has charge e and can move on the lattice. Coherent hopping of two hard-core bosons corresponds to a flipping process in the dimer model.

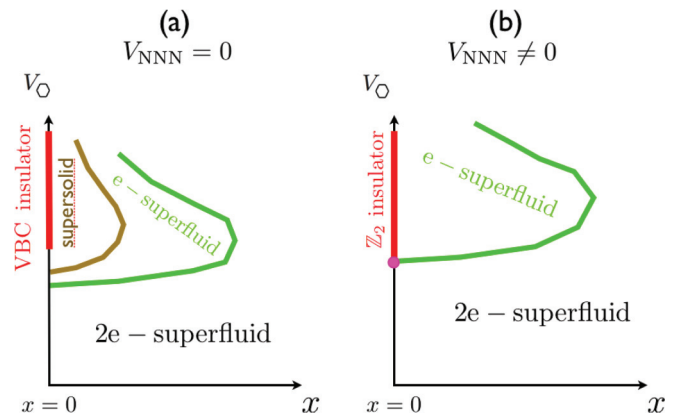


FIG. 12. (Color online) Schematic and speculative phase diagram of interacting HCB on the kagome lattice for $V_{dd} = 0$ (a), with fine tuning of the third-nearest-neighbor repulsion (b)—see text. In (a), the exact nature of the transitions between the $2e$ superconductor and the VBC insulator at $x = 0$ needs to be further investigated. In (b), the dot at $x = 0$ might correspond to the XY^* fractional critical point between the superfluid and the topological \mathbb{Z}_2 insulator. The charge- e superfluid is the same phase as in the doped QDM of Fig. 6(a).

to the QDM models (c) and (d) in the presence of a magnetic field. In practice only the case of a real $t < 0$ hopping on the original kagome lattice can be handled with QMC. Assuming the phase of the corresponding doped QDM [(a) model] is a fractionalized charge- e superfluid, we therefore predict a nonconventional phase transition between the (ordinary) charge- $2e$ superfluid of the weakly interaction d bosons and an exotic charge- e superfluid at large V_{\square}/t , as schematically shown in Fig. 12. This is possible if the third-nearest-neighbor repulsion is carefully tuned— $V_{\text{dd}} \simeq J = t^2/V_{\square}$. If $V_{\text{dd}} = 0$, one gets a transition to a plaquette VBC phase at $x = 0$, which might involve intermediate phases. Indeed, close similarities are expected with the melting of the (bosonic) plaquette VBC on the checkerboard lattice, revealing an intermediate commensurate supersolid.³¹ Similarly to the effective triangular QDM at $V = 0$, doping of the VBC insulator should immediately result in a supersolid phase which would melt into a charge- e superfluid above some critical doping. Last, at even larger doping (corresponding to a dilute gas of dimers) a second phase transition to a charge- $2e$ superfluid is expected.

VII. CONCLUSIONS AND DISCUSSIONS

In this paper we have established a rigorous and general equivalence between QDM Hamiltonians with bosonic holes and a corresponding QDM Hamiltonian with fermionic holes. Although this correspondence was already noticed on the basis of numerical simulations in Ref. 23 and established analytically in Ref. 18 for Hamiltonians with the simplest flipping term, the correspondence has now been generalized to more complicated cases. More importantly, we provide a general recipe to very quickly—and without any computation—establish, which are the two equivalent Hamiltonians under this statistical transmutation.

We also note that, when working with finite-size systems, while the composite particle representation is valid for any kind of boundary conditions, this is not the case for the method

that uses the Jordan-Wigner transformation. Indeed, the issue of boundary conditions in the two-dimensional version of the Jordan-Wigner transformation has been very little discussed in the literature. The point is that it does not seem possible to impose periodic boundary conditions in a consistent way when using the two-dimensional version of the Jordan-Wigner transformation, even if the total numbers of particles is kept fixed. This can be contrasted with the one-dimensional version of the transformation where periodic boundary conditions can be consistently imposed provided one keeps the number of particles fixed. In this sense the analytical results obtained¹⁸ with the help of the Jordan-Wigner transformation are only valid to infinite systems or a finite system with open boundary conditions while the composite particle representation used here can be consistently applied for any kind of boundary conditions. We have then provided many examples of equivalent Hamiltonians for the more generic cases of the square, triangular, hexagonal, and kagome lattices.

In order to detect condensation of fractionalized holons carrying charge e , we have introduced the gauge-invariant holon Green's function. We have then considered four inequivalent cases of QDM Hamiltonians on the triangular lattices and have numerically studied various correlation functions including the above-mentioned holon Green's function, by Lanczos exact diagonalization of finite-size clusters. We obtained rather strong and direct evidence for the existence of the exotic superfluid phase due to condensation of holons carrying charge e (charge- e superfluid phase), in terms of the behavior of the gauge-invariant holon Green's function. In fact, our numerical results suggest that all four models we have studied exhibit the charge- e superfluid phase. More conventional charge- $2e$ and $-4e$ superfluid phases are also present.

The existence of a charge- e superfluid phase may be naturally understood if the bare holes are bosons, which would then exhibit condensation. On the other hand, it is much more puzzling in the case where they are fermions, as it would correspond to a superconductor without Cooper pairing. While it might appear that the holes need to be bosons for the condensation of holons to take place, our rigorous mapping shows that fermionic statistics can be always assigned to holes in the microscopic Hamiltonian. This implies a dynamical statistical transmutation of holons in the QDM where holes are represented as fermions. Those kinds of dynamical statistical transmutations can be monitored by studying the nodes of the wave function and one spectacular example can be found in model (d) at intermediate values of the doping where the system seems to switch from a Fermi liquid to a (bosonic) charge- e superfluid phase.

We have then provided a concrete microscopic Bose-Hubbard Hamiltonian which in the strong interaction limit behaves as a QDM on the triangular lattice, as the one analyzed numerically. It allows us to have a better control on the doping (by simply varying the number of bosons) and to better visualize the different superfluid phases. It is important to stress that the same QDM may arise as an effective low-energy model of quite different microscopic Hamiltonians. As such, the physical consequences of various phases in the QDM can depend on the mapping. For example, if the QDM arises from a microscopic electronic Hubbard model, the holes are real electron vacancies [models (c) and (d)], and then they

are charged. In this case the different superfluid phases are superconducting phases.

There is, however, another way in which one could introduce doping. Imagine for example a system in which there are no real electron vacancies but some magnetic field is applied to the system. The applied magnetic field may have an effect to break some of the singlets that are represented by the dimers leaving two polarized spin $1/2$, which now play the role of the holes²⁴ [models (a) and (b)]. In this case the holes are neutral but carry spin, so that the superfluid phase now corresponds to a superconductor of magnetic current. Our results provide a validation of the previous claim²⁴ of an exotic superfluid of condensed deconfined and polarized spinons (equivalent to our charge- e superfluid). In addition, we predict here the existence of another phase of deconfined spinons, the Bose liquid, corresponding to an exotic spin liquid carrying *uncondensed* (polarized) spinons. Interestingly, such exotic phases could indeed be realized in simple frustrated magnetic systems, as for example the kagome anisotropic spin- $1/2$ model close to the magnetization plateau at $1/3$ of the saturation value.³²

One may question if the charge- e and charge- $2e$ superfluids discussed in the present paper actually represent distinct phases of matter, or if there is a smooth crossover connecting the two. While we do not have a mathematically rigorous proof at present, we believe that the long-distance asymptotic behavior of the gauge-invariant holon Green's function clearly distinguishes the charge- e superfluid from the conventional charge- $2e$ superfluid, in principle. Thus we expect a quantum phase transition separating these two distinct phases. On the other hand, being a nonlocal quantity, it appears difficult to measure the gauge-invariant holon Green's function in experiments. In order to characterize the charge- e superfluid experimentally, a different scheme such as the "vortex memory effect" discussed in Ref. 21 would be necessary.

We hope that the results of this paper will establish new motivations to investigate, with a new light, different microscopic models which may give rise to the doped QDM as an effective low-energy model.

ACKNOWLEDGMENTS

We are grateful to D. C. Cabra with whom we initiated the work in this subject. A.R., D.P., and P.P. acknowledge support by the "Agence Nationale de la Recherche" under Grant No. ANR 2010 BLANC 0406-0. M.O. was supported in part by Grant-in-Aid for Scientific Research on Innovative Areas No. 20102008 from MEXT of Japan. M.O. and D.P. were supported in part by the US National Science Foundation under Grant No. NSF PHY11-25915, while they were at Kavli Institute for Theoretical Physics, UC Santa Barbara. M.O. also thanks Aspen Center for Physics and NSF Grant No. 1066293 for hospitality supporting a part of the present work. C.A.L. was partially supported by CONICET (PIP 1691) and ANPCyT (PICT 1426).

APPENDIX: CONNECTION WITH THE TWO-DIMENSIONAL JORDAN-WIGNER TRANSFORMATION

In this Appendix we elaborate on an alternative proof of the statistical transmutation in the QDM. In this approach we use

a two-dimensional version of the Jordan-Wigner transformation. The fundamental ingredients of this transmutation were presented for the square and triangular lattices in a previous work.¹⁸ It is important to stress that this procedure is totally generic and can be implemented in any two-dimensional lattice with open boundary conditions.^{33,34} As the main technical steps for the square and triangular lattice were already presented in Ref. 18, here we only show the details for the kagome lattice. As we have discussed above, for this lattice there is a big freedom in choosing the ordering prescription. This fact gives rise to an extra freedom in taking the sign of the

flipping constants when we change the statistics of holes. We will see in this section that this freedom is materialized within the Jordan-Wigner approach by using gauge transformations on dimers and holes. Let us start with a quantum hard-core dimer model in the presence of holons on the kagome lattice given by the following Hamiltonian:

$$H = H_J + H_V + H_t. \quad (\text{A1})$$

The terms H_V and H_J corresponding to the diagonal and off-diagonal terms of the pure dimer model are taken up to resonance plaquettes of length 12.^{35,36}

$$H_J = J_6 \text{ (blue hexagon) } + J_8^{(a)} \text{ (blue 8-loop) } + J_8^{(b)} \text{ (blue 8-loop) } + J_8^{(c)} \text{ (blue 8-loop) } + J_{10}^{(a)} \text{ (blue 10-loop) } + J_{10}^{(b)} \text{ (blue 10-loop) } + J_{10}^{(c)} \text{ (blue 10-loop) } + J_{12} \text{ (blue 12-loop) } \quad (\text{A2})$$

$$H_V = V_6 \text{ (orange hexagon) } + V_8^{(a)} \text{ (orange 8-loop) } + V_8^{(b)} \text{ (orange 8-loop) } + V_8^{(c)} \text{ (orange 8-loop) } + V_{10}^{(a)} \text{ (orange 10-loop) } + V_{10}^{(b)} \text{ (orange 10-loop) } + V_{10}^{(c)} \text{ (orange 10-loop) } + V_{12} \text{ (orange 12-loop) } \quad (\text{A3})$$

The sum runs over all the hexagons of the lattice and all the possible orientations of the plaquettes are implicit. The kinetic and diagonal terms are given by

$$\begin{aligned} \text{Blue hexagon} &= \sum_{\Delta} \left\{ \left| \text{Blue 8-loop} \right\rangle \left\langle \text{Blue 8-loop} \right| + \text{H.c.} \right\} \\ \text{Orange hexagon} &= \sum_{\Delta} \left\{ \left| \text{Orange 8-loop} \right\rangle \left\langle \text{Orange 8-loop} \right| + \left| \text{Orange 10-loop} \right\rangle \left\langle \text{Orange 10-loop} \right| \right\} \end{aligned} \quad (\text{A4})$$

and similar expressions for the other terms. For convenience, the labels α in the amplitudes J_α and V_α correspond to the length of the associated resonance loops and when it corresponds to the three nonequivalent plaquettes for the cases of length 8 and 10. The Hamiltonian corresponding to the hopping of holons is given by

$$H_t = H_\Delta^{(t)} + H_\nabla^{(t)}, \quad (\text{A5})$$

where

$$\begin{aligned} H_\Delta^{(t)} &= -t \sum_{\Delta} \left\{ \left| \text{Blue 8-loop} \right\rangle \left\langle \text{Blue 8-loop} \right| + \left| \text{Orange 8-loop} \right\rangle \left\langle \text{Orange 8-loop} \right| + \left| \text{Orange 10-loop} \right\rangle \left\langle \text{Orange 10-loop} \right| \right. \\ &\quad \left. + \text{H.c.} \right\}. \end{aligned} \quad (\text{A6})$$

The hopping of holons can be written in a general way, independently of the lattice, as a sum of three-site Hamiltonians

$$H_t = \sum h_{(ijk)}^{(t)} \quad (\text{A7})$$

with

$$h_{(ijk)}^{(t)} = -t \hat{\mathcal{P}} b_{i,j}^\dagger b_{j,k} a_i^\dagger a_i \hat{\mathcal{P}}, \quad (\text{A8})$$

where we have projected the Hamiltonian on the subspace where the constraint

$$a_i^\dagger a_i + \sum_z b_{i,i+z}^\dagger b_{i,i+z} = 1 \quad (\text{A9})$$

is satisfied, where the sum runs over nearest neighbors of site i . Starting from $h_{(i,j,k)}^{(t)}$, we transform the boson operators a_i using

$$a_i = e^{-i\phi_i} f_i \quad (\text{A10})$$

with

$$\phi_i = \sum_{j \neq i} f_j^\dagger f_j \arg(\vec{\tau}_j - \vec{\tau}_i) \quad (\text{A11})$$

together with the following transformation for the dimer operators:

$$\tilde{b}_{i,j}^\dagger = b_{i,j}^\dagger e^{-i(\tilde{\phi}_i + \tilde{\phi}_j)}, \quad (\text{A12})$$

$$\tilde{b}_{i,j} = e^{i(\tilde{\phi}_i + \tilde{\phi}_j)} b_{i,j}, \quad (\text{A13})$$

we obtain

$$h_{(i,j,k)}^{(t)} = -\tilde{t} \hat{\mathcal{P}} \tilde{b}_{i,j}^\dagger \tilde{b}_{j,k} f_k^\dagger f_i \hat{\mathcal{P}}, \quad (\text{A14})$$

where the hopping amplitude is given by

$$\tilde{t} = t e^{i[\pi + \arg(\tau_j - \tau_i) - \arg(\tau_j - \tau_k)]}. \quad (\text{A15})$$

Equations (A14) and (A15) are, in fact, independent of the lattice details. The information concerning the lattice geometry is contained in the arguments on the exponential of Eq. (A15). This equation can be written in a compact form as

$$\tilde{t} = -t e^{i\psi_r}, \quad (\text{A16})$$

where $\psi_t = \arg(\tau_j - \tau_i) - \arg(\tau_j - \tau_k)$ can be represented graphically as

$$\psi_t = \begin{array}{c} k \\ \diagup \quad \diagdown \\ i \quad \rightarrow \quad j \end{array} - \begin{array}{c} k \\ \diagup \quad \diagdown \\ i \quad \leftarrow \quad j \end{array} \quad (\text{A17})$$

and $\begin{array}{c} k \\ \diagup \quad \diagdown \\ i \quad \rightarrow \quad j \end{array}$ represents the $\arg(\vec{\tau}_j - \vec{\tau}_i)$.

Now, we study the kinetic Hamiltonian corresponding to dimers. Let us start with the smallest resonance loop compatible with NN dimers on the kagome lattice, the plaquette of length 6. In this plaquette, the resonance of the two possible dimerizations is given by

$$H_{J_6} = J_6 \sum_{\Delta} \left\{ \left| \begin{array}{c} \text{Resonance 1} \\ \text{Resonance 2} \end{array} \right\rangle \left\langle \begin{array}{c} \text{Resonance 1} \\ \text{Resonance 2} \end{array} \right| + \text{H.c.} \right\}. \quad (\text{A18})$$

In order to transform the dimers to the new representation using the flux generated by the statistical transformation of the holons we write the Hamiltonian in terms of dimer operators $b_{i,j}$ as

$$H_{J_6} = \sum_{\Delta} h_{(i,j,k,l,m,n)}^{(J_6)} \quad (\text{A19})$$

with

$$h_{(i,j,k,l,m,n)}^{(J_6)} = J_6 b_{i,j}^\dagger b_{k,l}^\dagger b_{m,n}^\dagger b_{j,k} b_{l,m} b_{n,i} + \text{H.c.} \quad (\text{A20})$$

Using the transformation (A12) it is straightforward to write the Hamiltonian as

$$h_{(i,j,k,l,m,n)}^{(J_6)} = \tilde{J}_6 \tilde{b}_{i,j}^\dagger \tilde{b}_{k,l}^\dagger \tilde{b}_{m,n}^\dagger \tilde{b}_{j,k} \tilde{b}_{l,m} \tilde{b}_{n,i} + \text{H.c.}, \quad (\text{A21})$$

where

$$\tilde{J}_6 = -J_6 e^{i\psi_6} \quad (\text{A22})$$

and

$$\psi_6 = (\arg(\vec{\tau}_m - \vec{\tau}_n) + \arg(\vec{\tau}_i - \vec{\tau}_j) + \arg(\vec{\tau}_k - \vec{\tau}_l)) - ((\arg(\vec{\tau}_n - \vec{\tau}_i) + \arg(\vec{\tau}_j - \vec{\tau}_k) + \arg(\vec{\tau}_l - \vec{\tau}_m)).$$

It is convenient to use a graphical representation for the phase ψ_6


$$\psi_6 = \begin{array}{c} \text{Graph 1} \\ \text{Graph 2} \end{array} \quad (\text{A23})$$

where

$$\begin{array}{c} \text{Graph 1} \\ \text{Graph 2} \end{array} = (\arg(\vec{\tau}_m - \vec{\tau}_n) + \arg(\vec{\tau}_i - \vec{\tau}_j) + \arg(\vec{\tau}_k - \vec{\tau}_l))$$

$$\begin{array}{c} \text{Graph 3} \\ \text{Graph 4} \end{array} = ((\arg(\vec{\tau}_n - \vec{\tau}_i) + \arg(\vec{\tau}_j - \vec{\tau}_k) + \arg(\vec{\tau}_l - \vec{\tau}_m))$$

The two graphs correspond to the initial and final dimerization on the plaquette. In each graph we replace the dimers by arrows drawn in a clockwise direction and each graph represent the sum on the arguments of the arrows.

For the resonant plaquettes of length 8 we have three topologically distinct configurations. Let us study now the term corresponding to the resonance plaquette . After we write it in terms of dimer operators and transform following (A12) we obtain

$$\tilde{J}_8^{(b)} = -J_8^{(b)} e^{i\psi_8^{(b)}} \quad (\text{A24})$$

with

$$\psi_8^{(b)} = \begin{array}{c} \text{Graph 5} \\ \text{Graph 6} \end{array}, \quad (\text{A25})$$

where

$$\begin{array}{c} \text{Graph 5} \\ \text{Graph 6} \end{array} = (\arg(\vec{\tau}_m - \vec{\tau}_n) + \arg(\vec{\tau}_k - \vec{\tau}_l) + \arg(\vec{\tau}_i - \vec{\tau}_j) + \arg(\vec{\tau}_o - \vec{\tau}_p))$$

$$\begin{array}{c} \text{Graph 7} \\ \text{Graph 8} \end{array} = ((\arg(\vec{\tau}_n - \vec{\tau}_o) + \arg(\vec{\tau}_l - \vec{\tau}_m) + \arg(\vec{\tau}_j - \vec{\tau}_k) + \arg(\vec{\tau}_p - \vec{\tau}_i))$$

It is easy to check that, under transformation (A12) that the amplitudes $J_\alpha^{(y)}$ corresponding to the rest of the resonance plaquettes also transform as

$$\tilde{J}_\alpha^{(y)} = -J_\alpha^{(y)} e^{i\psi_\alpha^{(y)}}, \quad (\text{A26})$$

where $\psi_\alpha^{(y)}$ is the phase obtained from the difference between the two possible dimerizations in a given resonance plaquette of the sum of the arguments corresponding to dimers oriented clockwise (or anticlockwise).

This *graphical rule* can be used to study higher-order terms in the kinetic Hamiltonian. This allows us to determine the Hamiltonian after the JW transformation on the holons. In the kagome lattice, up to resonance plaquettes of length 12 we obtain that the Hamiltonian H_J corresponding to kinetic energy of the dimers can be written as in (A2), but dimers are now created by the operators $\tilde{b}_{i,j}^\dagger$ and the amplitudes J_α must be replaced by \tilde{J}_α whereas the values of V_α remains unchanged. In Table VI we show the values $\tilde{J}_\alpha/J_\alpha$ for the resonance plaquettes up to length 12.

After the transmutation the Hamiltonian corresponding to the hopping of holes is given by

$$\tilde{H}_t = \tilde{H}_\Delta^{(t)} + \tilde{H}_\nabla^{(t)}, \quad (\text{A27})$$

where in $\tilde{H}_\Delta^{(t)}$ dimers are also created by operators $\tilde{b}_{i,j}^\dagger$ and the holes are fermions created by the operators f_i^\dagger :

$$\tilde{H}_\Delta^{(t)} = -\tilde{t} \sum_{\Delta} \left\{ \left| \begin{array}{c} \text{Dimer 1} \\ \text{Dimer 2} \end{array} \right\rangle \left\langle \begin{array}{c} \text{Dimer 1} \\ \text{Dimer 2} \end{array} \right| + \left| \begin{array}{c} \text{Dimer 3} \\ \text{Dimer 4} \end{array} \right\rangle \left\langle \begin{array}{c} \text{Dimer 3} \\ \text{Dimer 4} \end{array} \right| + \left| \begin{array}{c} \text{Dimer 5} \\ \text{Dimer 6} \end{array} \right\rangle \left\langle \begin{array}{c} \text{Dimer 5} \\ \text{Dimer 6} \end{array} \right| \right\} + \text{H.c.}, \quad (\text{A28})$$

TABLE VI. Values of $\tilde{J}_\alpha/J_\alpha$ corresponding to the lowest orders of the resonant plaquettes.

Length	6		8	
ψ				
\tilde{J}/J	1	-1	1	-1
Length	10		12	
ψ				
\tilde{J}/J	1	-1	1	-1

where $\tilde{t} = t e^{-i(2/3)\pi}$. In order to obtain the original value of the hopping constant for the holons ($\tilde{t} \rightarrow t$), we can perform a gauge transformation on the dimers. This is possible, for example, the following gauge transformation:

$$\begin{aligned} |\bullet\bullet\rangle &\rightarrow |\bullet\bullet\rangle \\ |\bullet\circ\rangle &\rightarrow e^{-i\frac{2}{3}\pi} |\bullet\circ\rangle \\ |\circ\bullet\rangle &\rightarrow e^{i\frac{2}{3}\pi} |\circ\bullet\rangle, \end{aligned}$$

independently if the dimers are on up or down triangles. We have for the hole hopping term

$$\begin{aligned} \tilde{H}_\Delta^{(t)} = -t \sum_\Delta \left\{ \left| \begin{array}{c} \circ \\ \bullet \end{array} \right\rangle \left\langle \begin{array}{c} \bullet \\ \circ \end{array} \right| + \left| \begin{array}{c} \bullet \\ \circ \end{array} \right\rangle \left\langle \begin{array}{c} \circ \\ \bullet \end{array} \right| + \left| \begin{array}{c} \circ \\ \bullet \end{array} \right\rangle \left\langle \begin{array}{c} \bullet \\ \circ \end{array} \right| + \left| \begin{array}{c} \bullet \\ \circ \end{array} \right\rangle \left\langle \begin{array}{c} \circ \\ \bullet \end{array} \right| \right\} \\ + \text{H.c.} \end{aligned} \quad (\text{A29})$$

while for the resonance terms the gauge transformation does not change the couplings \tilde{J} and V . Then we obtain

$$\begin{aligned} \tilde{H}_J = J_6 &\begin{array}{c} \circ \\ \bullet \end{array} - J_8^{(a)} \begin{array}{c} \bullet \\ \circ \end{array} + J_8^{(b)} \begin{array}{c} \circ \\ \bullet \end{array} - J_8^{(c)} \begin{array}{c} \bullet \\ \circ \end{array} \\ + J_{10}^{(a)} &\begin{array}{c} \circ \\ \bullet \end{array} - J_{10}^{(b)} \begin{array}{c} \bullet \\ \circ \end{array} + J_{10}^{(c)} \begin{array}{c} \circ \\ \bullet \end{array} - J_{12} \begin{array}{c} \bullet \\ \circ \end{array} \end{aligned}$$

Finally we can use another gauge transformation to get a more simple Hamiltonian. We change the dimers on up triangles as

$$\begin{aligned} |\triangle\rangle &\rightarrow e^{i\theta_1} |\triangle\rangle \\ |\blacktriangle\rangle &\rightarrow e^{i\theta_2} |\blacktriangle\rangle \\ |\triangle\rangle &\rightarrow e^{i\theta_3} |\triangle\rangle \end{aligned}$$

while we change the corresponding down triangles as

$$\begin{aligned} |\blacktriangledown\rangle &\rightarrow e^{i\varphi_1} |\blacktriangledown\rangle \\ |\blacktriangledown\rangle &\rightarrow e^{i\varphi_2} |\blacktriangledown\rangle \\ |\blacktriangledown\rangle &\rightarrow e^{i\varphi_3} |\blacktriangledown\rangle \end{aligned}$$

Taking the values $\theta_1 = \theta_2 = \varphi_1 = \varphi_2 = 0$, $\theta_3 = \pi/2$, and $\varphi_3 = -\pi/2$, the amplitudes J_α change as

$$\begin{aligned} \tilde{H}_J = -J_6 &\begin{array}{c} \circ \\ \bullet \end{array} - J_8^{(a)} \begin{array}{c} \bullet \\ \circ \end{array} - J_8^{(b)} \begin{array}{c} \circ \\ \bullet \end{array} - J_8^{(c)} \begin{array}{c} \bullet \\ \circ \end{array} \\ - J_{10}^{(a)} &\begin{array}{c} \bullet \\ \circ \end{array} - J_{10}^{(b)} \begin{array}{c} \circ \\ \bullet \end{array} - J_{10}^{(c)} \begin{array}{c} \bullet \\ \circ \end{array} - J_{12} \begin{array}{c} \bullet \\ \circ \end{array} \end{aligned}$$

Then finally we obtain a Hamiltonian with a global change of sign in the amplitudes of the kinetic term. After the transformation, the terms corresponding to the hopping of holons becomes

$$\begin{aligned} \tilde{H}_\Delta^{(t)} = -t \sum_\Delta \left\{ e^{-i\pi/2} \left| \begin{array}{c} \circ \\ \bullet \end{array} \right\rangle \left\langle \begin{array}{c} \bullet \\ \circ \end{array} \right| \right. \\ \left. + \left| \begin{array}{c} \bullet \\ \circ \end{array} \right\rangle \left\langle \begin{array}{c} \circ \\ \bullet \end{array} \right| + e^{i\pi/2} \left| \begin{array}{c} \circ \\ \bullet \end{array} \right\rangle \left\langle \begin{array}{c} \bullet \\ \circ \end{array} \right| \right\} \\ + \text{H.c.} \end{aligned} \quad (\text{A30})$$

This hopping Hamiltonian can be transformed by mean a simple gauge transformation on the holes, $f_j \rightarrow e^{i\tilde{Q}\cdot\tilde{r}_j} f_j$ with $\tilde{Q} = (\frac{\pi}{2}, \frac{\pi}{2\sqrt{3}})$, to recover the original form of the Hamiltonian. With this transformation we have that

$$\begin{aligned} f_{j+p_1}^\dagger f_j &\rightarrow e^{i(\pi/2)} f_{j+p_1}^\dagger f_j, \\ f_{j+p_2}^\dagger f_j &\rightarrow e^{i(\pi/2)} f_{j+p_2}^\dagger f_j, \end{aligned}$$

and we recover the original form (A29) for the Hamiltonian corresponding to the holes. Then, finally we have that, changing the statistics of holons together with the sign of all the kinetic amplitudes, we obtain a completely equivalent Hamiltonian.

By using the JW transformation we can recover the equivalences presented in the previous section, but the procedure is more laborious. We have pointed out that starting from different prescriptions for the bonds we can prove different equivalences. A change in the lattice prescription used in the composite operator representation is equivalent to a gauge transformation on the dimers.

One last very important point concerns the issue of boundary conditions within the JW approach. The composite operator approach which we have extensively used in the paper is valid independently of the boundary conditions used for the system. In contrast, the JW approach is valid only for infinite systems or finite systems with open boundary conditions. Let us come back to Eq. (A10) assuming that the bosonic a operators are well defined in a system in periodic boundary conditions. This means that, for example, the operators a_i and $a_{\tilde{i}}$ are forced to be the same if sites i and \tilde{i} correspond to the same point in the system because of the periodic boundary

conditions. However, because of the very nature of the nonlocal JW transformation, the relation between the operators f_i and $f_{\tilde{i}}$ must contain a twist. In the one-dimensional version of the JW transformation, it is easy to see that this twist is a sign which depends only on the total number of particles in the system. Then, in one dimension, if one restricts to the subspace of a fixed number of particles it is possible to implement consistent periodic boundary conditions. Here in two dimensions, the

twist one should force for the fermionic operators depends not only on the number of particles but also on their relative positions with respect to the points i and \tilde{i} . That means that, even restricting to a fixed number of particles, starting from periodic boundary conditions for the bosons operators, it is not possible to implement boundary conditions for the fermionic operators which are consistent with all the possible particle configurations.

-
- ¹P. W. Anderson, *Science* **235**, 1196 (1987); *Mater. Res. Bull.* **8**, 153 (1973).
- ²D. S. Rokhsar and S. A. Kivelson, *Phys. Rev. Lett.* **61**, 2376 (1988).
- ³E. Manousakis and R. Salvador, *Phys. Rev. Lett.* **62**, 1310 (1989); S. Liang, *Phys. Rev. B* **42**, 6555 (1990).
- ⁴N. Read and S. Sachdev, *Phys. Rev. Lett.* **62**, 1694 (1989); S. Sachdev, *Phys. Rev. B* **40**, 5204 (1989); A. Ralko, D. Poilblanc, and R. Moessner, *Phys. Rev. Lett.* **100**, 037201 (2008); see also E. Fradkin, *Field Theories of Condensed Matter Systems* (Addison-Wesley, Redwood City, CA, 1991).
- ⁵R. Moessner and S. L. Sondhi, *Phys. Rev. Lett.* **86**, 1881 (2001).
- ⁶N. E. Bonesteel, *Phys. Rev. B* **40**, 8954 (1989).
- ⁷A. Yu. Kitaev, *Ann. Phys.* **303**, 2 (2003).
- ⁸M. Mambrini, A. Läuchli, D. Poilblanc, and F. Mila, *Phys. Rev. B* **74**, 144422 (2006).
- ⁹A. Ralko, M. Mambrini, and D. Poilblanc, *Phys. Rev. B* **80**, 184427 (2009).
- ¹⁰D. Poilblanc, M. Mambrini, and D. Schwandt, *Phys. Rev. B* **81**, 180402 (2010); D. Schwandt, M. Mambrini, and D. Poilblanc, *ibid.* **81**, 214413 (2010).
- ¹¹S. Yan, D. Huse, and S. White, *Science* **332**, 1173 (2011).
- ¹²H.-C. Jiang, Z. Wang, and L. Balents, *Nat. Phys.* **8**, 902 (2012).
- ¹³S. Depenbrock, I. P. McCulloch, and U. Schollwöck, *Phys. Rev. Lett.* **109**, 067201 (2012).
- ¹⁴E. Fradkin and S. Kivelson, *Mod. Phys. Lett. B* **4**, 225 (1990).
- ¹⁵M. Oshikawa and T. Senthil, *Phys. Rev. Lett.* **96**, 060601 (2006).
- ¹⁶N. Read and B. Chakraborty, *Phys. Rev. B* **40**, 7133 (1989); see also P. Lederer and Y. Takahashi, *Z. Phys. B* **71**, 311 (1988).
- ¹⁷S. Kivelson, *Phys. Rev. B* **39**, 259 (1989).
- ¹⁸C. A. Lamas, A. Ralko, D. C. Cabra, D. Poilblanc, and P. Pujol, *Phys. Rev. Lett.* **109**, 016403 (2012).
- ¹⁹D. J. Thouless, *Phys. Rev. B* **36**, 7187 (1987).
- ²⁰S. A. Kivelson, D. S. Rokhsar, and J. P. Sethna, *Europhys. Lett.* **6**, 353 (1988).
- ²¹T. Senthil and M. P. A. Fisher, *Phys. Rev. Lett.* **86**, 292 (2001).
- ²²D. A. Bonn, J. C. Wynn, B. W. Gardner, Y.-J. Lin, R. Liang, W. N. Hardy, J. R. Kirtley, and K. A. Moler, *Nature (London)* **414**, 887 (2001).
- ²³D. Poilblanc, *Phys. Rev. Lett.* **100**, 157206 (2008).
- ²⁴A. Ralko, F. Becca, and D. Poilblanc, *Phys. Rev. Lett.* **101**, 117204 (2008).
- ²⁵D. Poilblanc, F. Alet, F. Becca, A. Ralko, F. Trouselet, and F. Mila, *Phys. Rev. B* **74**, 014437 (2006).
- ²⁶A. Ralko, F. Mila, and D. Poilblanc, *Phys. Rev. Lett.* **99**, 127202 (2007).
- ²⁷A. Ralko, M. Ferrero, F. Becca, D. Ivanov, and F. Mila, *Phys. Rev. B* **71**, 224109 (2005).
- ²⁸M. Raczkowski and D. Poilblanc, *Phys. Rev. Lett.* **103**, 027001 (2009).
- ²⁹D. Poilblanc, *Phys. Rev. B* **44**, 9562 (1991).
- ³⁰S. V. Isakov, M. B. Hastings, and R. G. Melko, *Nat. Phys.* **7**, 772 (2011); S. V. Isakov, R. G. Melko, and M. B. Hastings, *Science* **335**, 193 (2012).
- ³¹A. Ralko, F. Trouselet, and D. Poilblanc, *Phys. Rev. Lett.* **104**, 127203 (2010); for the fermionic version, see D. Poilblanc, *Phys. Rev. B* **76**, 115104 (2007).
- ³²D. C. Cabra, M. D. Grynberg, P. C. W. Holdsworth, A. Honecker, P. Pujol, J. Richter, D. Schmalfluss, and J. Schulenburg, *Phys. Rev. B* **71**, 144420 (2005).
- ³³D. C. Cabra and G. L. Rossini, *Phys. Rev. B* **69**, 184425 (2004).
- ³⁴C. A. Lamas, D. C. Cabra, M. D. Grynberg, and G. L. Rossini, *Phys. Rev. B* **74**, 224435 (2006).
- ³⁵D. Poilblanc and A. Ralko, *Phys. Rev. B* **82**, 174424 (2010).
- ³⁶C. Zeng and V. Elser, *Phys. Rev. B* **51**, 8318 (1995).